3D groundwater flow and deformation modelling of Madrid aquifer

Roberta Bonì [1],*, Claudia Meisina[1], Pietro Teatini[2], Francesco Zucca[1], Claudia Zoccarato[2], Andrea Franceschini[2], Pablo Ezquerro[3], Marta Béjar-Pizarro[3], José Antonio Fernández-Merodo[3], Carolina Guardiola-Albert[3], José Luis Pastor[4], Roberto Tomás[4], Gerardo Herrera[3]

[1] Department of Earth and Environmental Sciences, University of Pavia, Via Ferrata 1, Pavia 27100, Italy; roberta.boni01@universitadipavia.it; claudia.meisina@unipv.it; francesco.zucca@unipv.it

[2] Department of Civil, Environmental and Architectural Engineering, University of Padua, via Marzolo 9, 35131 Padua (PD), Italy;pietro.teatini@unipd.it; claudia.zoccarato@unipd.it; franc90@dmsa.unipd.it

[3] Geohazards InSAR Laboratory and Modeling Group, Instituto Geológico y Minero de España (IGME), C/. Alenza 1, 28003 Madrid, Spain; p.ezquerro@igme.es; m.bejar@igme.es; jose.fernandez@igme.es; c.guardiola@igme.es; g.herrera@igme.es

[4] Universidad de Alicante, Dpto. de Ingeniería Civil, Escuela Politécnica Superior de Alicante, P.O. Box 99, 03080 Alicante, Spain; joseluis.pastor@ua.es; roberto.tomas@ua.es

* Correspondence roberta.boni01@universitadipavia.it; Tel.: +39 0382985842

Abstract: A novel methodological approach to calibrate and validate three-dimensional (3D) finite element (FE) groundwater flow and geomechanical models has been implemented using Advanced Differential Interferometric SAR (A-DInSAR) data. In particular, we show how A-DInSAR data can be effectively used to (1) constrain the model set-up in evaluating the areal influence of the wellfield and (2) characterise the aquifer system, specifically the storage coefficient values, which represents a fundamental step in managing groundwater resources. The procedure has been tested to reconstruct the surface vertical and horizontal movements caused by the Manzanares-Jarama wellfield located northwest of Madrid (Spain). The wellfield was used to supply freshwater during major droughts over the period between 1994 and 2010. Previous A-DInSAR outcomes obtained by ERS-1/2 and ENVISAT acquisitions clearly revealed the seasonality of the land displacements associated to the withdrawal and recovery cycles that characterized the wellfield development. A time-lag of about one month, which is in the order of the time span between two SAR acquisitions, between the hydraulic head changes and the displacements has been detected in this site by a wavelet analysis of A-DInSAR and piezometer time series. The negligible delay between the forcing factor and the system response and the complete subsidence recovery when piezometric head recovers supported the understanding of a minor role played by the pore pressure propagation within clay layers and the almost perfectly elastic behavior of the system (viscosity is negligible), respectively. The developed geomechanical model satisfactorily reproduces the pumping-induced deformations with a Root Mean Square Error (RMSE) between observed and simulated land displacements in the order of 0.1-0.3 mm. The results give insights about the approach benefits in deeply understanding the spatio-temporal aquifer-system response to the management of this strategic water resource for Madrid.

Keywords: seasonal deformation; land subsidence; 3D Finite Element (FE) groundwater and geomechanical model; A-DInSAR technique; groundwater management

1. Introduction

One of the most evident impacts related to the long-term aquifer over-exploitation is land subsidence. The loss of land elevation can be permanent if the lowering of the groundwater level causes the increase of the effective stress above the pre-consolidation value, with a partial rebound that follows the recovery of the groundwater level after the reduction of groundwater overuse (Galloway *et al.* 1998). Furthermore, a withdrawal rate exceeding some sustainable limits can lead to a permanent loss of aquifer capability to store water because of soil mechanical hysteresis (Béjar-Pizarro *et al.,* 2017). The development of modelling tools to predict impacts and plan efficient and sustainable strategies is a key requirement for improving the management of groundwater resources. Three-dimensional (3D) models of complex aquifers allow understanding the behavior in time and space of the flow and pressure fields, as well as the interaction between different geological layers (Teatini *et al.* 2006; Martínez-Santos *et al.* 2010; Ye *et al.* 2016; Ezquerro *et al.* 2017; Ochoa-González *et al.* 2018). However, 3D models require an adequate knowledge of the subsurface to set-up a realistic conceptual model of the system and a huge amount of geological, hydrogeological (i.e. aquifer properties, piezometric level variations and pumping rates during the monitored period) and geomechanical information to provide reliable responses.

To overcome the lack of direct *in-situ* data, commonly occurring in regional hydrogeological studies, advanced analyses have recently taken advantage of satellite-based methods. Retrieving processes occurring on the land surface can allow an indirect characterization of the subsurface parameters of interest. In particular, land movements obtained by Advanced Differential Interferometric Synthetic Aperture Radar (A-DInSAR) techniques have been used to quantify aquifer related deformation, estimate aquifer hydraulic properties, and model hydraulic head at well locations (Galloway *et al.* 1998; Erban *et al.* 2014; Ezquerro *et al.* 2014; Chaussard *et al.* 2014; Chen *et al.* 2016; Béjar-Pizarro *et al.* 2017; Bonì *et al.* 2017; Li and Zhang 2018; Choopani *et al.* 2019; Rezaei and Mousavi 2019). Hoffmann *et al.* (2003) exploited InSAR-derived subsidence observations to implement an inverse procedure for the estimate of the deformation time constant and inelastic skeletal storage coefficient of compacting interbeds to be used in a regional groundwater flow and aquifer-system subsidence model of the Antelope Valley (California). They used InSAR data to calibrate a MODFLOW subsidence model (McDonald *et al.* 1988) and validate the numerical results. Herrera *et al.* (2009) demonstrated the potential of A-DInSAR techniques to calibrate and validate subsidence model predictions by comparing the temporal evolution of the displacements observed in Murcia (Spain) with the values computed using the GeHoMadrid finite element code (Fernandez-Merodo 2001). Calderhead *et al.* (2011) extended the approach introduced by Hoffmann *et al.* (2003) by using A-DInSAR subsidence measurements to constrain a groundwater flow-compaction analysis with a 3D geologic model in the Toluca Valley (Mexico). In these cases, the authors used a one-dimensional (1D) modelling approach to simulate the aquifer system compaction and land subsidence due to piezometric level drawdown. Three-dimensional (3D) approaches have been used in studies related to land subsidence due to hydrocarbon production from deep reservoirs. Teatini *et al.* (2011a) described the improved results obtained by the use of A-DInSAR data to calibrate a 3D flow model and a 3D transversally isotropic geomechanical model to simulate the land displacements caused by underground gas storage in depleted hydrocarbon reservoirs. With reference to the calibration of parameters to be used in 3D geomechanical models, Fokker *et al.* (2016) described the application of A-DInSAR data to estimate subsurface model parameters for the Bergermeer gas field (Netherlands).

In this framework, the integration of A-DInSAR technique proved a valuable contribution to calibrate and validate reliable models implemented with different approaches. Besides the evident advances, there is still a lack of exhaustive and complete studies on the use of the A-DInSAR technique as supporting tool for groundwater management strategies, even more dealing with a 3D framework. The compound challenges now faced by water planners require a new generation of more efficient models for aquifer management, addressing the changes of aquifer storage, and to analyze the response

of the groundwater system to various stresses (natural versus anthropogenic pressure). For this reason, the aim of this work is to develop a methodological approach to characterise the aquifer behavior by integrating A-DInSAR data and 3D numerical groundwater flow analyses and by giving insight about the A-DInSAR data support for 3D geomechanical modelling. The methodology has been tested on the Manzanares-Jarama wellfield located in the northwest area of Madrid (Spain). The aquifer represents a strategic water resource for the most populated city of Spain, which is vulnerable to drought as recently experienced over a number of important dry periods. Between 1994 and 2010 the wellfield was used to cope with three major droughts, interrupted by periods of well shutdown sufficiently long to recover the original piezometric level in the aquifer. Therefore, the study area represents a perfect example to test the integrated methodological approach proposed in the work. The developed geomechanical model allows to infer a more precise estimate of the aquifer compressibility and storage using ground surface deformation. The results could be used to develop appropriate strategies for a sustainable management of the Madrid aquifer in view of even more frequent droughts because of the expected climate changes.

2. Geological and hydrogeological setting of the study area

The study area is a portion of the large Tertiary detritic aquifer (TDAM, around 2,500 km^2) situated in the northwest of Madrid, Spain, comprising the Manzanares-Jarama wellfield (Figure 1). The wellfield is located in the intermontane tectonic depression of the Madrid basin that is bounded by Paleozoic granitic and schists rocks of the Sierra of Guadarrama in the northern sector and by the evaporitic materials in the southern part (Hernández-García and Custodio, 2004). The deposits at the boundaries are less permeable than the aquifer soils (Heredia *et al.* 2001; Navarro Alvargonzález *et al.* 1993). The western and eastern boundaries are the alluvial deposits of the Manzanares and Jarama rivers. The Manzanares river drains this part of the basin, contributing to the Jarama river.

The aquifer is constituted by continental Tertiary detrical deposits and a Quaternary coverage (Martínez-Santos *et al.* 2010). The sourcing area of the sediments is the Sierra of Guadarrama made by gneiss and granites. These deposits formed an alluvial fan, with the aquifer that is formed by arkosic sand lenses embedded in clayey and silty deposits (Hernández-García and Custodio 2004). The TDAM is a heterogeneous multi-layer system characterized by a thickness from 200 to 2000 m (Vera *et al.* 1982; Martínez-Bastida *et al.* 2010). The regional trend of the aquifer permeability shows an increase towards SE (Ezquerro et al. 2014).

The study area covers approximately 540 km^2, with an elevation ranging from 500 to 800 m a.s.l. and it is exploited by 32 wells. Quaternary deposits, which are composed by sand and clay, overlap upper Tertiary deposits such as Oligocene and lower Miocene sediments composed by gravel, clay and calcareous rocks. The deep Tertiary deposits are Cretaceous and Paleozoic deposits (Figure 1c). Available piezometric measurements acquired by 17 piezometers from 1998 to 2012 show three major extraction phases coinciding with drought periods (Yélamos, and Villarroya, 1991) followed by recovery periods and a last extraction phase not as pronounced as the previous ones (Figure 1d). Most of the wells are between 400 and 500 m depth and piezometers are located at 50 and 300 m depth. Since the most productive layers are characterized by local lateral changes, the wells are screened along the whole borehole length to intercept the most productive sandy lenses. Because the upper 100 m of the aquifer-system is more susceptible to local depletion, the shallowest screens are usually located below that depth.

The regional flow conditions are locally modified by various factors, for example due to the topography of the basin, its complex geometry, and the anisotropic nature of aquifer materials (Martínez-Santos et al. 2010, Cordoba 2012). Taking into account that no other well fields with similar depth and productivity exist in the area surrounding the study site, it is possible to exclude significant interactions with the rest of the aquifer.

3. A-DInSAR analysis

Available Synthetic Aperture Radar (SAR) image stacks consist of 50 ERS-1/2, and 31 ENVISAT scenes. The monitored periods by ERS-1/2 and ENVISAT spanned from April 1992 to November 2000 and between August 2003 and September 2010, respectively. The ERS-1/2 data were acquired along the descending orbit and the ENVISAT images in ascending mode. The datasets were processed through PSP-IFSAR technique (Costantini *et al.* 2008). The average incidence angle of the two sensors is 23° from the vertical direction. Additional information about the SAR images are provided in Table 1 and in the supplementary material.

The unavailability of ascending or descending datasets spanning a common period did not allow the decomposition of the line of sight (LOS) ground motion into the vertical and horizontal components. By assuming that the displacements are mainly vertical across the study area, LOS displacements and velocities for both datasets were projected along the vertical direction dividing the LOS measurements by the cosine of the incidence angle.

As observed by previous authors (Ezquerro *et al.* 2014; Béjar-Pizarro *et al.* 2017), the deformation area is localized within a 6-km buffer zone around the wells. It is worth noting the lack of targets in the central zone of the study site due to the presence of vegetation coverage that precludes the coherence of the radar signal.

During the monitoring period from 1992 to 2000 and from 2003 to 2010, various groundwater extraction and recovery periods were observed (Ezquerro *et al.* 2014; Béjar-Pizarro *et al.* 2017). The LOS displacements (mm) during the different extraction and recovery periods were computed. In particular, two representative extraction periods were analysed, including the time intervals from February 1999 to March 2000 and from April 2005 to October 2006 and two recovery periods from January 1996 to January 1999 and between December 2006 and September 2010 (Figure 2).

4. Methods

The geomechanical response of an aquifer system to pressure changes can be characterized by different constitutive relationships such as elastic, elasto-plastic, and visco-elasto-plastic (Zhang *et al.* 2007). Moreover, the complex nature of the aquifer system, specifically the presence of fine compressible layers and lenses where the pressure variation can be delayed relative to that in the aquifers, is usually associated to a temporal shift of the displacement field relative to the pressure evolution. Therefore, a preliminary analysis of the relationship between piezometric changes and land subsidence can provide useful suggestions to adopt the most appropriate geological and geomechanical models for the hydrogeological characterization of an aquifer system.

In this paper, continuous wavelet tools were used to analyze the relationship between the land movements observed using A-DInSAR and groundwater level changes observed in the piezometric time-series. Then, the A-DInSAR-based measurements are properly used to constrain the 3D numerical groundwater flow and geomechanical models. Specifically, the joint use of A-DInSAR data and hydraulic head changes allowed to set the areal dimension of the simulated domain, characterize the aquifer properties, and select the most suitable geomechanical constitutive law to simulate the aquifer deformation. In the following sections the various components of the proposed methodology are described in detail.

4.1 Wavelet method

Continuous Wavelet Transform (CWT) is used for the analysis of individual time series. This tool allows finding localized intermittent periodicities in non-stationary processes expanding the time series into time frequency space. CWT result is depicted as a two-axis plot defined by the time (X-axis) and the period of the time patterns (Y-axis), in which the areas exhibiting high values indicate the presence of significant time patterns (i.e. seasonality) at particular dates.

Complementarily, other methods as Cross Wavelet Transform (XWT) and Wavelet Coherence (WTC) allow the joint analysis of the CWT of two-time series in order to identify their common power and relative phase in time-frequency space, and to find significant coherence even though the common power is low, respectively (Grinsted *et al.* 2004). XWT is calculated as the product between the CWT of the first time-series and the complex conjugate of the CWT of the second time-series (Grinsted *et al.* 2004). The result is depicted as a 2-D plot of complex numbers whose absolute value will be high in the time-frequency areas of the representation in which both CWT display high values, indicating the existence of common time patterns between both datasets. Additionally, the phase (i.e. the angle of the vectors) of the XWT provides the time shift between the two time-series.

WTC is computed as the coherence between the two CWT. It is defined as the normalized cross-correlation between them, including a smoothing operator that operates in time and frequency or scale domains (Grinsted *et al.* 2004). The interpretation of the result of WTC is similar to that of XWT, although the resolution degrades. For further details about these methods the user should consult the works published by Grinsted *et al.* (2004) and Torrence and Compo (1998).

In this work, we used the approach developed by Tomás *et al.* (2016) for the application of wavelet tools to A-DInSAR and piezometric level time series. The first step consisted in equalizing the spacing in time of the two time-series. We used a 35 days interval that matches the revisit interval of ERS and ENVISAT satellites. Linear interpolation between the two closest images was used to fill the gap for the missing acquisition dates in order to avoid the introduction of false periods into the analysis. The second step consisted in the separation of the linear and non-linear components of the displacement time series at each well where the analysis was performed. The cyclical behaviors are defined by the non-linear component of the A-DInSAR time-series. To this aim, a linear regression of the time series records was carried out and the non-linear component was calculated as the difference between the original time-series and the fitted linear component. In the third step, the piezometric time series were also equally spaced in time linearly interpolating values for the same dates of the A-DInSAR time series. As previously explained, the linear and non-linear components of the time series were separated.

Finally, the CWT was separately applied to the A-DInSAR and the piezometric levels time series to identify cyclic and seasonal characteristics in the frequency domain. Subsequently, XWT and WTC permitted the recognition of the common power, the relative phase in time-frequency space, and the significant coherence and confidence levels against Brownian noise backgrounds between the A-DInSAR and piezometric levels time series. Additionally, the phase difference ($\Delta\phi$) allows quantifying the temporal shift (Δt) between the two time series (i.e. land subsidence and piezometric level) for each period (T), identified from the XWT and CWT analysis, through the equation:

$$\Delta t = \frac{\Delta\phi \times T}{2\pi} \tag{1}$$

Because of the used time interval (i.e. 35 days), the identification of cyclicities with a time period equal or longer than this value was possible.

4.2 Methodology for the implementation of the 3D model

A methodology is here proposed to integrate A-DInSAR-based measurements with 3D numerical groundwater flow and geomechanical models (Figure 3).

The procedure consists of three main phases. In the first phase, the geologic model, also defined as "static" model, is built up and discretized into finite elements. In the second phase, the groundwater flow model is implemented using

hydrogeological information and aquifer storage parameters derived from piezometric and A-DInSAR records. Finally, the third step is focused on the implementation of the geomechanical model using A-DInSAR data to calibrate the soil compressibility. Compressibility and specific storage must assume consistent values.

Phase I. Geological model setup. A three-dimensional finite element (FE) grid of the selected domain is constructed using GEN3D (Teatini *et al.* 2006). This code is a 3D mesh generator that initially projects a two-dimensional (2D) triangular mesh into tetrahedra and, subsequently, uses different transformations such as translation, mapping, removal of degenerated (null volume) elements to adjust the node locations in order to match the geological information, also in the presence of lenses, faults, and layer pinch-out.

Firstly, a 2D Delaunay mesh of the domain horizontal extent has been generated using Argus One (Argus Holdings Ltd, 2011). A uniform discretization routine is used to generate a homogeneously-spaced node distribution along linear features representing the domain boundary and inner zone limits. Then, control vertices are inserted around selected various features (e.g., the wells) in order to enforce the discretization in specific locations of the model domain. Once the 2D mesh is available, GEN3D is used to construct the 3D mesh. In particular, the inputs for the 3D mesh generation are the 2D grid, including the node coordinates and the triangle topology, the bounds of possible sub-domains and a number of layers representing the elevation of ground level surface and the other surfaces of interest such as the top and bottom of the various geologic units (aquifers and aquitards), and the depth of the domain basement. Furthermore, the number of FE layers selected to refine the vertical discretization of each geologic unit has to be specified.

Phase II. Groundwater flow model. The SAT3D (SATurated Three-Dimensional) simulator is used to develop the groundwater flow model (Teatini *et al.* 2006). SAT3D uses 3D finite elements and an implicit Euler method to compute the piezometric evolution due to anthropogenic and natural forcing factors in transient conditions, taking into account the possible variation of the soil storage with pressure values (Gambolati *et al.* 1999; Gambolati *et al.* 2000; Teatini *et al.* 2011b). More precisely, the hydrodynamic of the aquifer is computed using the groundwater flow equation introduced by Bear (1972):

$$\nabla(\boldsymbol{k} \cdot \nabla h) = S_s \cdot \frac{\partial h}{\partial t} + q \tag{2}$$

where $\boldsymbol{k}$ and h are the hydraulic permeability tensor and the hydraulic head, respectively, t is time, and q is the source/sink term The specific storage (S_s) of the confined aquifer is computed dividing the storativity by the aquifer thickness (b) as follows (Fetter, 2001):

$$S_s = \frac{S}{b} \tag{3}$$

The aquifer storativity (S) is defined as the sum of the bulk storage (S_k) and the water storage (S_w). The different deformation behavior of the soil to stress induced by the hydraulic head variations is described using two different bulk storage, i.e. inelastic or plastic (S_{kv}) and elastic (S_{ke}) in loading and unloading/reloading conditions, respectively. Taking into account that in compacting aquifer systems $S_k \gg S_w$ (Poland, 1984), the storativity is equal to the bulk storage, e.g. $S \approx S_{ke}$ in unloading re-loading conditions. In this work, the elastic storage (S_{ke}) is computed by applying a methodology implemented by several authors, using A-DInSAR-based and extensometers-based displacement measurements (Sneed and Galloway, 2000; Burbey, 2003; Zhang *et al.* 2007; Tomás *et al.* 2010; Bonì *et al.* 2016). The following equation is used to estimate the elastic storage:

$$S = S_{ke} = \frac{\Delta d}{\Delta h} \tag{4}$$

6

where Δd is the aquifer compaction caused by a Δh piezometric level decrease. The vertical displacement is measured using A-DInSAR measurements and the piezometric level change is derived from the piezometric head time series. Equation (4) holds when the soil deformation is mainly vertical. This condition always holds for aquifers and reservoirs experiencing pore pressure change except where faults/fractures/geologic discontinuities can be responsible for significant horizontal strain (e.g., Ye et al., 2018). Therefore, it is fully warranted for the TDAM aquifer. The inputs to the groundwater flow model are the hydrogeological parameters of the aquifer such as the permeability, the specific storage, and the porosity. The parameters are assumed homogeneous within each layer of the model. Furthermore, the initial and boundaries conditions must be prescribed, together with the amount of groundwater extracted from the wells at each time step of the simulation. The results of this phase in terms of piezometric evolution are cross-compared with the available piezometric measurements.

Phase III. Geomechanical Model.

After a preliminary calibration of the groundwater flow model, the geomechanical model is applied. Indeed, the incremental pore pressure variation ($p = \gamma \cdot \Delta h$; where γ represents the specific weight of water) induced by water pumping over the simulated time span is the input to the geomechanical model. In particular, the SUB3D code (Teatini *et al.* 2006) is used to compute the incremental displacement field $\boldsymbol{u}$ along the x, y, and z directions. Assuming an elastic isotropic medium, the equilibrium equations (Verruijt, 1969):

$$G\nabla^2 u_i + (\lambda + G)\frac{\partial \varepsilon}{\partial i} = \frac{\partial p}{\partial i} \qquad i = x, y, z \tag{5}$$

are solved, where λ and G are the Lamé constant and shear modulus of porous medium, respectively, $\varepsilon = \frac{\partial u_x}{\partial x} + \frac{\partial u_y}{\partial y} + \frac{\partial u_z}{\partial z}$ is the volume strain, and u_i the displacement component estimated along the i-th coordinate direction.

Notice that:

$$G = \frac{E}{2(1 + \nu)} \tag{6}$$

with E the Young modulus and ν the Poisson ratio.

The soil compressibility (c_M) is related to E and ν through the well-known relation:

$$c_M = \frac{(1 + \nu)(1 - 2\nu)}{E(1 - \nu)} \tag{7}$$

It is worth noting that S_s can be defined as:

$$S_S = \gamma \cdot (c_M + \varphi \cdot \beta) \tag{8}$$

where φ is the soil porosity, and β the volumetric fluid compressibility of the water.

4.3 Component integration and model calibration

The three phases described above are properly integrated for calibration purposes. The same static model developed in phase 1 is consistently used in the flow (phase 2) and geomechanical (phase 3) models. Indeed, great care has been devoted to the gridding issues as suggested by Settari *et al.* (2005). A major advantage of using SAT3D and SUB3D is that the same tetrahedral grid developed by the mesh generator is used in both the ground water flow and geomechanical

computation. This allows avoiding approximations related to the need of interpolating the pressure changes from the mesh of the flow model to that used in the geomechanical simulation.

The calibration of hydrogeological and geomechanical parameters is carried out by a traditional trial and error approach. Notice that water flow in a confined aquifer system is more influenced by the hydraulic permeability than the specific elastic storage. Conversely, the displacement field computed by the equilibrium equations are linearly dependent (in poro-elasticity) to E, and therefore c_M. Consequently, the model calibration has required an iterative procedure to guarantee a consistent soil compressibility (c_M) value in the two modelling phases. Based on the above notes, the following steps have been implemented (Figure 3): a) SAT3D is initially run using the S_s value derived through Equations (3) and the hydraulic conductivity from the literature review (Torrego, 2012), then a trial and error procedure has been performed to calibrate k by matching the groundwater flow model results with the available piezometric records; b) the piezometric changes are converted to pressure changes and used as source term to run SUB3D; c) the geomechanical model is calibrated using a trial and error procedure to set E , and consequently c_M, by reproducing the A-DInSAR displacement measurements. If the calibrated c_M differs more than a threshold ξ from the value obtained using equation (8), a new iteration (a) to (c) is needed with SAT3D that is re-run by adopting the oedometric compressibility calibrated by SUB3D and this latter by using the updated pressure change. Based on previous experiences (Teatini *et al.* 2006; Teatini *et al.* 2011b; Ochoa-González *et al.* 2018;), ξ=10% has been used in this study.

5. Results

5.1 Wavelet analysis of A-DInSAR and piezometric time series

The wavelet analysis was carried out for 17 piezometers established in the Manzanares-Jarama wellfield. The relative phase in time-frequency space (Δϕ) has been quantified and the temporal gaps (Δt) between land subsidence and piezometric levels time series have been calculated using equation (1) for each period recognized in the WTC analysis.
The wavelet analysis for two representative wells, FA-1 and FE-1, over the time interval spanned by ENVISAT is shown in Figure 4. The results in terms of CWT of individual time series of piezometric level show two significant periodicities (thick lines in the time-frequency plots) of 1 and 2 years for 2005-2007 and 2006-2008, respectively. The 2-year period characterized by the higher power according to the colour scale. It is worth noting that the colour scale represents the significance level of wavelet power (as a percentage) against Brownian noise and is considered significant for values higher than 5%. Finally, a lower significant periodicity of near half a year can be recognized from the middle 2005 to 2007 in the piezometric time series. In the case of CWT of A-DInSAR time series, two significant 1- and 2-year periodicities can be also identified from 2005 to 2007 and 2006-2008, respectively. These results indicate that groundwater level and displacements mainly exhibit 1- and 2-year oscillations during the above described periods.
XWT and WTC, which are computed from pairs of CWTs of piezometric levels and A-DInSAR displacements time series, show some regions with high common cross-wavelet power and coherence, respectively. In detail, XWT cross-power spectrums enable the identification of strong common cross-wavelet power for 1- and 2-year periods for the time spans 2005-2007 and 2006-2008, respectively. The same conclusions are achieved from the analysis of the WTC scalograms. Therefore, XWT and WTC have enabled to identify potential physical relationships between piezometric level and InSAR displacements time series.
The first signal identified corresponds to the 1-year seasonal natural changes (winter-summer cycles). The second signal corresponds to the 2-year drought periods. It is the period during which the groundwater resources were extracted from the wellfield because of lack of rainfall. It can also be observed that the vectors in the WXT and WTC panels in

correspondence of these two periods point rightward and have a small angle relative to the positive horizontal axis. This means that the two signals are in-phase, and thus there exist a short time lag between the two time-series (A-DInSAR displacements and piezometric level). The results for the 17 wells are summarised in Table 2, providing similar results for all wells. The mean time lag (Δt) for the 1-year period amounts to 1.0±0.6 months, with minimum and maximum values equal to 0.0 and 3.3 months, respectively. The piezometer FA-3 shows no delay and 65% of the analysed piezometers is characterized by a delay lower than 1 month. Similarly, the minimum and maximum lags for the 2-year period are 0.2 and 3.2 months, respectively, with a mean value equal to 1.4±0.9 months. In all but one analysed case, the direction of the arrows in XWT scalograms indicates that land subsidence is always anticipated by groundwater level decline. It is worth noting that FE-1R is the unique time series of the 17 analysed pairs of time series in which XWT provided a delay of piezometric level against land subsidence (i.e. that land subsidence starts before that piezometric level falls). Obviously, this delay made not physical sense and is the result of the bad quality of the analysed data as observed in the original time series (i.e. the raw data) of FE-1R.

The spatial investigation reveals that the time delay is a little longer in the northern sector of the study area. For this period, 41% of the analysed piezometers is characterized by a delay lower than 1 month (Table 2).

This outcome suggests that clayey units within the aquifer system play a minor role since no significant consolidation delay is observed. Furthermore, time series show that subsidence totally recovers when the piezometric head recovers and, thus, a purely elastic geomechanical behaviour of the porous medium can been assumed to simulate the deformation in the Manzanares-Jarama wellfield.

5.2 3D static model

The first phase of the 3D modelling was aimed to reconstruct the 3D static model representing the hydrogeological structure of the study area. The model includes the upper 700 m of the aquifer system, with the domain that is bounded at the top by the ground surface extracted from the 5-m pixel digital elevation model by Instituto Geográfico Nacional (IGN) (http://centrodedescargas.cnig.es/CentroDescargas/index.jsp) and the bottom by the Lower Miocene unit depth (IGME, 1989; IGME, 2000). Although the available stratigraphic information reveals a complex geological setting (Ezquerro *et al.* 2014), the lack of information to define a detailed 3D geological model has suggested to simplify the structure into three main hydrogeological units. Specifically, the units correspond to the upper phreatic aquifer, an intermediate aquitard, and the lower confined aquifer. This latter represents the portion of the system mainly exploited for water supply. It is characterized by heterogeneous sediments made of sandy lens embedded in clayed soils (Ezquerro *et al.* 2014). The numerous relatively-thin low-permeability lenses and layers within the elevation from 300 to 400 m a.s.l. have been represented by a single continuous clayey unit reducing the hydraulic connection between the upper and the lower aquifers at the Manzanares-Jarama wellfield.

The domain extends horizontally to include a 10-km wide buffer ring around the wellfield (Figure 1a). Previous investigations (Ezquerro *et al.* 2014) revealed that the piezometric drawdown caused by the wells did not reach this distance. The domain is discretized by a 3D FE mesh consisting of 137,646 nodes and 769,386 tetrahedral elements. An initial plane Delaunay mesh made up of about 15,000 triangles and 7,650 nodes was vertically projected and adapted to the actual geologic structure to obtain the final 3D grid. The upper aquifer, intermediate aquitard, and lower aquifer are represented by a number of 10, 2, and 5 layers of FEs, respectively (Figure 5). The grid resolution in the horizontal plane is increased in proximity of the wells, with the element characteristic dimension decreasing from 500 m at the lateral boundary to 150 m in the nearby of the wellfield. The modeling calibration was mostly focused on the confined aquifer (lower aquifer), with the withdrawals from the unconfined aquifer (upper aquifer) being negligible.

5.3 Groundwater flow model

The groundwater flow model was applied to simulate the aquifer dynamic during the period from 1994 to 2010 (Figure 6). The behaviors of the piezometric level observed at the Manzanares-Jarama wellfield are strictly correlated with the wellfield management. Since 1994, the wellfield operated during four 1-1.5 year long periods, i.e. from March 1995 to December 1995, February 1999 to March 2000, March 2002 to December 2002, and between April 2005 and November 2006 corresponding with drought periods in central Spain. The prolonged groundwater abstraction triggered a quick lowering of the piezometric level ranging from 100-120 m to 250 m. Because of the large drawdown, the periods of groundwater extraction were alternated with recovery intervals, when the aquifer piezometric level naturally returned almost to the original undisturbed condition (Figure 7).

From the modelling point of view, the total amount of the groundwater withdrawal made available by the water company (Figure 6) was equally divided between the production wells (Canal de Isabel II Gestión, 2014; Iglesias Martín, 2011). Therefore, the withdrawal rates were reproduced in the model through Neumann conditions. The domain bottom was assumed as a no-flow boundary, similarly to the land surface since the exploited aquifer cannot be directly recharged by rainfall or river leakage because of the large depth and the presence of clayey levels. Moreover, as the model aims to represent the deep aquifer dynamics, groundwater flow in the upper part of the aquifer system (e.g. rainfall recharge or evapotranspiration) are neglected. A fixed head was assumed along the lateral boundary due to the large distance from the wellfield. The 16-year simulation period was divided into monthly time steps.

As suggested by Ezquerro *et al.* (2014), the (elastic) specific storage of the confined aquifer was initially estimated using Equations (3) and (4) through A-DInSAR measurements, and using literature data as proposed by Younger (1993) for the shallower formation. Regarding the hydraulic conductivity, the data reported by Hernández Torrego (2012) and the interpretation of pumping tests performed at the piezometer CB5 were used to compute the initial values. A one order of magnitude modification has been suggested by the calibration procedure for the hydraulic conductivity of the deep aquifer. The calibrated values of hydraulic conductivity are provided in Table 3. The simulated heads agree satisfactorily with the observed levels (Figure 7). The withdrawal and recovery cycles are adequately captured and also the peak values are well reproduced, with. the difference increasing a bit over the last recovery period i.e. starting from 2006. The absolute error and the standard deviation between the simulated hydraulic head changes and the observed values are reported for all piezometers in Table 4. It is worth noting that the percentage error respect to the maximum drawdown of the groundwater extraction cycles ranges from 5.9 to 17.5% with an average value of 9.1 % (Table 4). The average absolute error between the simulated and observed hydraulic head reaches 11.2 m with a standard deviation of 9.3 m.

5.4 Geomechanical deformation model

The piezometric changes were used as input data in the geomechanical model. The calibrated geomechanical parameters are provided in Table 3, with *E*=247.6 MPa in the pumped aquifer. The Poisson's ratio *v* was set to 0.3, which is a common value for sedimentary deposits (Teatini *et al.* 2006). Standard Dirichlet conditions were assumed, with a fixed basement, the horizontal displacements precluded on the outer boundaries, and the top surface that was left free to move both vertically and horizontally.

The results of the simulation give insight about the vertical and horizontal component of the land displacement during the different periods of groundwater extraction and piezometric recovery. During the period from January 1996 to January 1999 (Figure 8a) the recovery of the groundwater level triggers an uplift mainly encompassing the wellfield. An area of about 178 km^2 experienced a rise larger than 20 mm. During the same period, horizontal west-east displacement up to 5 mm also developed because of piezometric recovery (Figure 8e). The spatial pattern of the movements is

10

characterized by westward (i.e., negative values) and eastward (i.e., positive values) movements to the west and east part of the wellfield barycenter, respectively. During the period from February 1999 to March 2000, the groundwater extraction caused a land subsidence that amounted to more than 20 mm over an area of about 190 km^2 (Figure 8b). Regarding the horizontal movements, the maximum simulated displacements amounted to about 6 mm with a pattern of the westward and eastward movements that are reversed with respect to the previous period (Figure 8f). Similar outcomes were obtained over the following extraction (from April 2005 to October 2006, Figures 8c and 8g) and piezometric recovery (between December 2006 and September 2010, Figures 8d and 8h) periods.

Unfortunately, no observations for the horizontal displacements are available, because SAR images were acquired with a single acquisition geometry only. It is worth noting that a discussion on the effect of the boundaries conditions on the model bottom is provided in section 6.3.

6. Discussion

6.1 Forcing factor vs aquifer deformation

A specific approach to integrate A-DInSAR data and 3D numerical model of soil deformations caused by groundwater withdrawal was proposed and applied to the case of Manzanares-Jarama wellfield. The Manzanares-Jarama wellfield is a unique case study for its peculiarity in relation to the well distribution and the withdrawal behavior versus time. In fact, the wellfield is made by a clustered group of wells far away from any other source potentially contributing to land subsidence in the area. The results of a preliminary wavelet analysis revealed a time delay of about one month between the piezometric fluctuation and A-DInSAR displacement time series. Furthermore, the analysis of the A-DInSAR time series pointed out a fully recovery of land subsidence when the piezometric head naturally returned to the original values shortly after the well shutdown. Therefore, the use of an elastic mechanical relationship and a simplified hydrogeological setting was totally justified.

The short time delay between the forcing factor (groundwater pumping) and the system response (land displacements) for the study aquifer system are likely due to a minor role played by the fine-texture layers, which limits (1) the viscous/creep behavior and (2) the delayed drainage typical of thick, compressible and low-permeable aquitards.

Indeed, significant time delay was previously recognized in various aquifers such as the San Joaquin Valley and Antelope Valley in USA, Shanghai in China (Wu *et al.* 2010), and the Alto Guadalentin basin in Spain (Bonì *et al.* 2015). For example, in the case of the San Joaquin Valley, a viscoelastic aquifer model was proposed by Corapcioglu *et al.* (1977) to simulate land subsidence in order to take into account the plasticity and creep behavior of sandy-clay layers within the aquifer system. In the Antelope Valley, the time lag was associate to a slowly drainage where the pore fluid pressure did not instantaneously equilibrate with the head because of compressible interbeds characterized by a low vertical hydraulic conductivity (Hoffmann *et al.* 2003). More in-depth studies are surely required to clarify the mechanisms related to the time delay deformation response of the aquifer system at the Manzanares-Jarama wellfield.

6.2 Comparison between the simulated displacements and the satellite-based measures

The displacement time series simulated by means of the 3D numerical model of the Manzanares-Jarama wellfield have been compared with the displacement measured by the A-DInSAR technique. The comparison was performed using the movements at the mesh nodes corresponding to the piezometer locations and the average LOS displacement time series measured on the persistent scatterers (PS) located within a 1000-m radius buffer zone around the piezometers. Because the piezometers are characterized by similar groundwater level variations over time (Figure 1c), two

representative monitoring points (i.e. FE-1 and FA-) were selected for the comparison. The extension of the buffer area around the well was chosen considering the influence zone of the wells (Ezquerro *et al.* 2014). At piezometer FE-1, the absolute difference between the simulated and the observed measurements ranges from 0.5 to 32.2 mm, with an average difference and a standard deviation of 10.4 and 8.3 mm, respectively (Figure 9). The values of the Root Mean Square Error (RMSE) are of 0.3 and 0.1 mm for the measurements simulated at the piezometer FE-1 and FA-1, respectively. The estimate error is comparable with that obtained by Ezquerro *et al.* (2014) in the simulation of the land displacement for the Madrid aquifer using a one-dimensional approach.

At the piezometer FA-1, the absolute difference amounts to an average value of 10.5 mm and a standard deviation equal to 7.7 mm. The maximum and minimum absolute difference between the simulated and the observed measurements are 28.1 and 0.1 mm, respectively.

Figure 10 provides the simulated land displacements versus the corresponding observed measurements at the two selected piezometers. The distribution of the points highlights the generally good agreement between the two data sets for both the piezometers. The absolute average difference of 11.6 mm and 8.8 mm over the ERS and ENVISAT period, respectively, are evaluated at piezometer FE-1. At piezometer FA-1, the model outcome shows an average absolute difference of 13.0 mm and 9.1 mm with the ERS and ENVISAT measurements, respectively (Figure 10).

Furthermore, Figure 11 shows the spatial pattern of the absolute difference between the simulated vertical displacements and the A-DInSAR measurements for a few cycles of groundwater extraction and recovery. The model outcome at the PS locations has been directly obtained using the linear basis functions the tetrahedral FE discretization. This comparison approach has been chosen because the study area is characterized by vegetated zones where A-DInSAR measurements are not available, as already noted in section 3. During the period from January 1996 to January 1999, the differences are limited with an average and standard deviation equal to 8.0 and 6.2 mm, respectively (Figure 11a). Larger differences are obtained mainly during the extraction periods from February 1999 to March 2000 (Figure 11b) and from April 2005 to October 2006 (Figure 11c). A zone of about 13 km^2, located in the south-western part of the study area, is characterized by an average difference of 25 mm (Figure 11b) and 30 mm (Figure 11c). This can be attributed by the Pozuelo de Alarcón wellfield, a secondary group of wells located to the north-west of Madrid (Figure 1), whose effect was not accounted for in this study. From December 2006 to September 2010, the differences are approximately 20 mm in area of around 25 km^2 along the Manzanares river (Figure 11d).

Globally, an absolute difference smaller than 15 mm was computed for about 87% and 80% of the measuring points over the periods from January 1996 to January 1999 and from December 2006 to September 2010, respectively. Similarly, the percentage amount to 80% and 75% from February 1999 to March 2000 and between April 2005 and October 2006, respectively.

6.3 Effects of boundary conditions on the geomechanical model response

Previous studies (e.g., Burbey, 1999; Burbey and Helm, 1999) already highlighted the importance of investigating the 3D pattern of the stress and deformation fields associated to groundwater pumping, with horizontal displacements. In fact, the use of a 3D modelling configuration improves significantly the capability of understanding the geomechanical response of an exploited aquifer system. The advantage is counterbalanced by the need to characterize a larger number of parameters and more complex boundary conditions. About these latter, a major role can be played by the displacement prescribed on the model bottom. Usually, when a traditional 3D flow plus 1D compaction approach is used:

- the lateral extent of the simulated domain is selected sufficiently large as required by the flow model to reduce the boundary effect on the zone of major interest;

- the model basement is selected in correspondence of the bottom of the deepest pumped aquifer where no-flow condition and null vertical displacement are prescribed in the hydrologic and geomechanical model, respectively.

This second choice can affect significantly the 3D displacement field since the condition is imposed directly on the bound of the depleted unit. In particular, the condition on the horizontal displacements needs a specific investigation, although also the null vertical displacement of the aquifer bottom could be a rough approximation only (Geertsma, 1973).

For this reason, a second simulation has been performed where the bottom was kept free to move horizontally (Figure 12). The results of the simulations obtained with the previous modelling set-up and the new boundary condition on the model bottom are shown in Figures 13 and 14: the vertical and horizontal (west-east) movements are provided along a vertical section and for one of the piezometric borehole. It is worth noting that the two boundary conditions provide west-east movements with maximum values that differ of about one order of magnitude. If the model bottom is free to move horizontally, the maximum value of the easting displacement of the land surface is comparable to land subsidence. Also notice that a certain difference, even though much smaller than that for the horizontal movements, is computed for the land subsidence too. Because of the three-dimensionality of the deformation field, limiting the horizontal contraction yields a larger vertical compaction. Obviously, the "exact" solution is intermediate between the two outcomes here presented as the deposits below the aquifer exert a resistance to the lateral contraction of the depleted layer because of their intrinsic stiffness. Unfortunately, no measurements of the horizontal movements are available at the date for the study area.

To remove this ambiguity, in the geomechanical simulation of land deformation due to hydrocarbon production or deep fluid injection (e.g., Teatini *et al.*, 2011a, 2011b) where 3D analysis is mandatory, the model basement is usually placed well below the reservoir/aquifer bottom, with the discretization of a thick underburden that removes the effect of the arbitrarily selected boundary condition on the model solution.

7. Conclusions

The characterization of a portion of the Madrid aquifer has been performed for the first time by implementing a 3D one-way coupled numerical model where the pore pressure changes as provided by the fluid-dynamic model are imposed as volumetric loads in the geomechanical model and an iterative cycle is implemented to guarantee the consistency of the soil compressibility value in the two models. The calibration of the hydromechanical parameters has been achieved using a trial and error procedure, which is nested within the iterative cycle implemented to guarantee the compressibility consistency. A-DInSAR measurements were exploited to estimate the aquifer storage and to calibrate the geomechanical model results. The use of geomechanical model allowed improving the estimate of soil compressibility, and therefore specific storage. Indeed, the groundwater flow model outcome is mainly controlled by the hydraulic conductivity values rather than the specific storage and the calibration makes use of the piezometric measurements. Conversely, the response of the geomechanical model is directly proportional to compressibility values, taking the maximum advantaged from A-DInSAR measurements of land displacement. Therefore, the specific storage values retrieved by the geomechanical model calibration are more accurate than the values obtained using only a groundwater flow model.

The aquifer system dynamics was characterized for the period 1994-2010, including cycles of withdrawal and recovery. The aquifer response to groundwater pumping and natural recharge was fast showing land subsidence during the extraction phase, coinciding with the drought periods and uplift in the recovery phase. Indeed, the analysis of the piezometers and A-DInSAR displacements time series using the wavelet tools gives insight of about one month of the time delay between the hydraulic head changes and the deformation. Furthermore, the groundwater flow and

geomechanical models suggest that the displacement field is characterized by a horizontal component which cannot be identified using A-DInSAR data acquired using a single viewing geometry. The comparison of the computed land movements and the displacements measured using A-DInSAR shows that the model outcome agree well with the observed measurements, capturing the minimum and maximum peak values and the seasonality of the behavior.

The methodology shows the benefits of A-DInSAR solutions to support the characterization of aquifer properties over large areas in order to compensate the lack of in-situ hydrogeological data. Three-dimensional (3D) modelling is crucial to understand the aquifer behavior, including the vertical and horizontal component of ground motion. Overall, the obtained results could be used by the groundwater authorities to adopt sustainable strategies for the management of groundwater resources and to predict the aquifer response to future pumping periods in the Madrid area.

Author Contributions: R.B. built the three-dimensional numerical modeling for the Manzanares-Jarama wellfield and prepared the manuscript in the framework of the post-doc project. C.M. provided support and guidance throughout the research process for the geological interpretation of the data. P.T. provided a guidance to build the groundwater flow and geomechanical models and he contributed to the analysis of the results. C.Z. and A.F. from UniPD supported the development of the groundwater flow and geomechanical models. F.Z. supported the numerical modeling and the interpretation of the results. G.H. provided the geological, the hydrogeological and A-DInSAR data and supported their analysis. P.E. and M.B. from IGME supply the geological and hydrogeological interpretation of the study area. A.J.F supported the interpretation of the geomechanical model. C.G. provided a guidance for the interpretation of the groundwater flow model. RT and JLP performed the wavelet analysis. All authors co-wrote and reviewed the manuscript.

Conflicts of Interest: The authors declare no conflict of interest.

References

Argus Holdings Ltd. [Argus], 2011 Argus Holdings Ltd. [Argus], 2011. Argus ONE, Israel. Available at: http://www.argusint.com/index.html (Date of access: 21st May 2019).

Bear, J. Dynamics of fluids in porous materials. *Society of Petroleum Engineers: Dallas*, 1972, TX, USA.

Béjar-Pizarro, M., Ezquerro, P., Herrera, G., Tomás, R., Guardiola-Albert, C., Hernández, J. M. R., Fernández Merodo, J. A., Marchamalo, M. Martínez, R. 2017. Mapping groundwater level and aquifer storage variations from InSAR measurements in the Madrid aquifer, Central Spain. *Journal of Hydrology*, 547, 678-689.

Bonì, R., Cigna, F., Bricker, S., Meisina, C., McCormack, H. 2016. Characterisation of hydraulic head changes and aquifer properties in the London Basin using Persistent Scatterer Interferometry ground motion data. *Journal of Hydrology*, 540, 835-849.

Bonì, R., Herrera, G., Meisina, C., Notti, D., Béjar-Pizarro, M., Zucca, F., González, P.J., Palano, M., Tomás, R., Fernández, J., Fernández-Merodo, J.A., Mulas, J., Aragón, R., Guardiola-Albert, C., Mora, O., 2015. Twenty-year advanced DInSAR analysis of severe land subsidence: the Alto Guadalentín Basin (Spain) case study. *Engineering Geology*, 198, 40-52.

Bonì, R., Meisina, C., Cigna, F., Herrera, G., Notti, D., Bricker, S., McCormack, H., Tomás, R., Béjar-Pizarro, M., Mulas, J. and Ezquerro P. 2017. Exploitation of satellite A-DInSAR time series for detection, characterization and modelling of land subsidence. *Geosciences*, 7, 25.

Burbey, T.J. 1999. Effects of horizontal strain in estimating specific storage and compaction in confined and leaky aquifer systems. Hydrogeology Journal, 7(6), 521-532.

Burbey, T.J. 2003. Use of time-subsidence data during pumping to characterize specific storage and hydraulic conductivity of semiconfining units. *Journal of Hydrology,* 281, 3-22.

Burbey, T.J., and Helm, D.C. 1999. Modeling three-dimensional deformation in response to pumping of unconsolidated aquifers. Environmental and Engineering Geoscience, 5(2), 199-212.

Calderhead, A. I., Therrien, R., Rivera, A., Martel, R., and Garfias, J. 2011. Simulating pumping-induced regional land subsidence with the use of InSAR and field data in the Toluca Valley, Mexico. *Advances in Water Resources*, 34(1), 83-97.

Canal de Isabel II Gestión, 2014. Captación de aguas de superficie y subterraneas. Technical report. (in Spanish).

Chaussard, E., Bürgmann, R., Shirzaei, M., Fielding, E. J., Baker, B. 2014. Predictability of hydraulic head changes and characterization of aquifer-system and fault properties from InSAR-derived ground deformation. *Journal of Geophysical Research: Solid Earth*, 119(8), 6572-6590.

Chen, J., Famigliett, J. S., Scanlon, B. R., Rodell, M. 2016. Groundwater storage changes: present status from GRACE observations. In *Remote Sensing and Water Resources*, pp. 207-227, Springer, Cham.

Choopani, A., Dehghani, M., Nikoo, M.R. 2019. Determining hydrogeological parameters of an aquifer in Sirjan Basin using Envisat ASAR interferometry and groundwater modelling. *International Journal of Remote Sensing*, 1-28.

Corapcioglu, M. Y., & Brutsaert, W. 1977. Viscoelastic aquifer model applied to subsidence due to pumping. *Water Resources Research*, 13(3), 597-604.

Córdoba, D. 2012. Utilización de herramientas de información geográfica para la integración en modelos hidrogeológicos. Master Thesis.

Costantini, M., Falco, S., Malvarosa, F., Minati, F. 2008. A new method for identification and analysis of persistent scatterers in series of SAR images. In Geoscience and Remote Sensing Symposium, 2008. IGARSS 2008. *IEEE International* 2008, Vol. 2, pp. II-449). IEEE.

Erban, L.E., Gorelick, S.M., Zebker, H.A. 2014. Groundwater extraction, land subsidence, and sea-level rise in the Mekong Delta, Vietnam. *Environmental Research Letters*, 9(8), 084010.

Ezquerro, P., Guardiola-Albert, C., Herrera, G., Fernández-Merodo, J. A., Béjar-Pizarro, M., Bonì, R. 2017. Groundwater and subsidence modeling combining geological and multi-Satellite SAR data over the Alto Guadalentín Aquifer (SE Spain). *Geofluids*, 2017.

Ezquerro, P., Herrera, G., Marchamalo, M., Tomás, R., Béjar-Pizarro, M., Martínez, R. 2014. A quasi-elastic aquifer deformational behavior: Madrid aquifer case study. *Journal of Hydrology*, 519, 1192-1204.

Fernandez Merodo, J. A. 2001. Une approche a la modelisation des glissements et des effondrements de terrains: Initiation et propagation (Thesis), Ecole Centrale Paris, 2001.

Fetter, C.W. Applied hydrogeology (4th Edition).2001. Upper Saddle River: Prentice hall.p.102. ISBN 0-13-088239-9.

Fokker, P. A., Wassing, B. B. T., van Leijen, F. J., Hanssen, R. F., and Nieuwland, D. A. 2016. Application of an ensemble smoother with multiple data assimilation to the Bergermeer gas field, using PS-InSAR. *Geomechanics for Energy and the Environment*, 5, 16-28.

Galloway, D. L., Hudnut, K. W., Ingebritsen, S. E., Phillips, S. P., Peltzer, G., Rogez, F., Rosen, P. A. 1998. Detection of aquifer system compaction and land subsidence using interferometric synthetic aperture radar, Antelope Valley, Mojave Desert, California. *Water Resources Research*, 34(10), 2573-2585.

Gambolati, G., Putti, M., Paniconi, C. 1999. Three-dimensional model of coupled density-dependent flow and miscible salt transport. *In Seawater intrusion in coastal aquifers—Concepts, methods and practices*, pp. 315-362. Springer Netherlands.

Gambolati, G., Teatini, P., Baú, D., Ferronato, M. 2000. Importance of poroelastic coupling in dynamically active aquifers of the Po river basin, Italy. *Water Resources Research*, 36(9), 2443-2459.

Geertsma J. 1973. Land subsidence above compacting oil and gas reservoirs. *J. Petroelum Technolgy*, 25, 734–744.

Grinsted, A., Moore, J.C. Jevrejeva, S. 2004. Application of the cross wavelet transform and wavelet coherence to geophysical time series. *Nonlin. Processes Geophys.*, 11, 561-566.

Heredia, J., Martín-Loeches, M., Rosino, J., Del Olmo, C., Lucini, M. 2001. Síntesis hidrogeológica y modelización regional de la cuenca media del Tajo asistida por un SIG. *Estudios Geológicos*, 57(1-2), 31-46.

Hernández Torrego, E. 2012. La recarga profunda de agua en las masas 003-010 y 003-011 del acuífero detrítico terciario de la fosa del Tajo (Madrid), PhD thesis.

Hernández-García, M. E., Custodio, E. 2004. Natural baseline quality of Madrid Tertiary Detrital Aquifer groundwater (Spain): a basis for aquifer management. *Environmental Geology*, 46(2), 173-188.

Herrera, G., Fernández, J. A., Tomás, R., Cooksley, G., Mulas, J. 2009. Advanced interpretation of subsidence in Murcia (SE Spain) using A-DInSAR data-modelling and validation. *Nat. Hazards Earth Syst. Sci.*, 9(3), 647-661.

Hoffmann, J., Galloway, D. L., Zebker, H. A. 2003. Inverse modeling of interbed storage parameters using land subsidence observations, Antelope Valley, California. *Water Resources Research*, 39(2).

http://centrodedescargas.cnig.es/CentroDescargas/index.jsp (Date of access: 21st May 2019).

Iglesias Martín J. A. 2011. Aplicación de la recarga artificial al acuífero terciario detrítico de Madrid por medio de pozos profundos: experiencias de Canal de Isabel II. *Technical report*, 2011**.**

IGME 1989. Geological Map of Spain, region 559. Technical report. (in Spanish). Available at: http://info.igme.es/cartografiadigital/geologica/Magna50Hoja.aspx?id=559#memoria_y_metadatos (Date of access: 21st May 2019).

IGME 1995. Mapa Geológico de la Península Ibérica, Baleares y Canarias a escala 1:1.000.000, edición 1995. https://servicio.mapama.gob.es/sia/visualizacion/descargas/mapas.jsp (Date of access: 21st May 2019).

IGME 2000. Geological Map of Spain, region 534. Technical report. (in Spanish). Available at: http://info.igme.es/cartografiadigital/geologica/Magna50Hoja.aspx?Id=534#memoria_y_metadatos (Date of access: 21st May 2019).

Li, L., Zhang, M. 2018. Inverse modeling of interbed parameters and transmissivity using land subsidence and drawdown data. *Stochastic Environmental Research and Risk Assessment*, 32(4), 921-930.

Martínez-Bastida, J. J., Arauzo, M., Valladolid, M. 2010. Intrinsic and specific vulnerability of groundwater in central Spain: the risk of nitrate pollution. *Hydrogeology Journal*, 18(3), 681-698.

Martínez-Santos, P., Pedretti, D., Martínez-Alfaro, P. E., Conde, M., Casado, M. 2010. Modelling the effects of groundwater-based urban supply in Low-permeability aquifers: application to the Madrid Aquifer, Spain. *Water resources management*, 24(15), 4613-4638.

McDonald, M. G., Harbaugh, A. W. 1988. A modular three-dimensional finite-difference ground-water flow model (Vol. 6, p. A1). Reston, VA: US Geological Survey.

Navarro Alvargonzález, A., Fernández Uría, A., Dobles Domínguez, J. G. Cuenca del Tajo, 1993. Las aguas subterráneas en España. Ed. Instituto Geológico y Minero de España, Madrid. 1993, Cap. IX, 217-230.

Ochoa-González, G. H., Carreón-Freyre, D., Franceschini, A., Cerca, M., Teatini, P. 2018. Overexploitation of groundwater resources in the faulted basin of Querétaro, Mexico: A 3D deformation and stress analysis. *Engineering Geology*, 245, 192-206.

Poland, J.F. 1984. Guidebook to studies of land subsidence due to ground-water withdrawal. Unesco, Paris, France.

Rezaei, A., Mousavi, Z. 2019. Characterization of land deformation, hydraulic head, and aquifer properties of the Gorgan confined aquifer, Iran, from InSAR observations. *Journal of Hydrology*, 124196.

Settari, A., Walters, D. A., Stright Jr, D. H., Aziz, K. 2008. Numerical techniques used for predicting subsidence due to gas extraction in the North Adriatic Sea. *Petroleum Science and Technology*, 26(10-11), 1205-1223.

Sneed, M., Galloway, D.L. 2000. Aquifer-system compaction and land subsidence: measurements, analyses, and simulations: the Holly site, Edwards Air Force Base, Antelope Valley, California. *US Geol Surv Water-Resour Invest Rep*, 00-4015. 65 pp.

Teatini, P., Castelletto, N., Ferronato, M., Gambolati, G., Janna, C., Cairo, E., Marzorati, D., Colombo, D., Ferretti, A., Bagliani, A. Bottazzi, F. 2011a. Geomechanical response to seasonal gas storage in depleted reservoirs: A case study in the Po River basin, Italy. *Journal of Geophysical Research: Earth Surface*, 116(F2).

Teatini, P., Ferronato, M., Gambolati, G., Gonella, M. 2006. Groundwater pumping and land subsidence in the Emilia-Romagna coastland, Italy: Modeling the past occurrence and the future trend. *Water Resources Research*, 42(1).

Teatini, P., Ferronato, M., Gambolati, G., Baù, D., Putti, M. 2011b. Anthropogenic Venice uplift by seawater pumping into a heterogeneous aquifer system. *Water Resour Res*, 46, W11547.

Tomás, R., Herrera, G., Lopez-Sanchez, J.M., Vicente, F., Cuenca, A., Mallorquí, J.J. 2010. Study of the land subsidence in Orihuela City (SE Spain) using PSI data: Distribution, evolution and correlation with conditioning and triggering factors. *Engineering Geology,* 115, 105–121.

Tomás, R., Li, Z., Lopez-Sanchez, J.M., Liu, P. Singleton, A. 2016. Using wavelet tools to analyse seasonal variations from InSAR time-series data: a case study of the Huangtupo landslide. *Landslides*, 13, 437-450.

Torrence, C. and Compo, G.P. 1998. A Practical Guide to Wavelet Analysis. *Bulletin of the American Meteorological Society*, 79, 61-78.

Vera, F. L., Lerman, J. C., Muller, A. B. 1982. The Madrid basin aquifer: Preliminary isotopic reconnaissance. *In Developments in Water Science*, Vol. 16, pp. 151-166, Elsevier.

Verruijt, A. 1969. Elastic storage of aquifers, *in: Flow Through Porous Media*, edited by: De Wiest, R., Elsevier, NY, 331–376.

Wu, J., Shi, X., Ye, S., Xue, Y., Zhang, Y., Wei, Z., Fang, Z. 2010. Numerical simulation of viscoelastoplastic land subsidence due to groundwater overdrafting in Shanghai, China. *Journal of Hydrologic Engineering*, 15(3), 223-236.

Ye, S., Luo, Y., Wu, J., Yan, X., Wang, H., Jiao, X., Teatini, P. 2016. Three-dimensional numerical modeling of land subsidence in Shanghai, China. *Hydrogeology Journal*, 24(3), 695-709.

Ye, S., Franceschini, A., Zhang, Y., Janna, C., Gong, X., Yu, J., Teatini, T. 2018. A novel approach to model earth fissure caused by extensive aquifer exploitation and its application to the Wuxi case, China. *Water Resources Research*, 54, doi:10.1002/2017WR021872.

Yélamos, J. G., Villarroya, F. I. 1991. Variación de la piezometría y el caudal en cuatro explotaciones de aguas subterráneas en el acuífero del Terciario detrítico de Madrid. *Bol. Geol. Min*, 102(6), 857-874.

Younger, P. L. 1993. Simple generalized methods for estimating aquifer storage parameters. Quarterly Journal of Engineering Geology and Hydrogeology, 26(2), 127-135.

Zhang, Y., Xue, Y.-Q., Wu, J.-C., Ye, S.-J., Li, Q.-F. 2007. Stress–strain measurements of deforming aquifer system that underlie Shanghai, China. Environ. *Eng. Geosci.*, XIII, 217–228.

Tables

Table 1. SAR data and processing details.

Satellite	ERS-1/2	ENVISAT
Sensor's band	C-band	C-band
Orbit	Desc.	Asc.
look angle (º)	23	23
Time span	1992-2000	2003-2010
Processing technique	PSP-IFSAR	PSP-IFSAR
N° scenes	50	31

Table 2. Periods and relative phase derived from wavelet analysis of the InSAR and piezometric time series of the wells of the study area.

Well	Period, T (years)	Time lag, Δt (months)	Well	Period, T (years)	Time lag, Δt (months)
CA-3	-	-	**CA-3**	2	3.2
CA-4	1	0.3	**CA-4**	2	0.8
CA-5	1	0.6	**CA-5**	2	0.8
CB-5	1	3.3	**CB-5**	2	2.8
CB-6	1	0.7	**CB-6**	2	1.7
CB-9	1	0.6	**CB-9**	2	1.5
CB-11	1	1.4	**CB-11**	2	1.0
CB-12	1	0.2	**CB-12**	2	2.4
CB-13	1	0.2	**CB-13**	2	2.2
CB-14	1	0.9	**CB-14**	2	1.2
CB-15	1	1.2	**CB-15**	2	0.8
FA-1	1	0.9	**FA-1**	2	1.3
FA-3	1	0.0	**FA-3**	2	0.6
FC-2	1	1.0	**FC-2**	2	0.2
FE-1	1	2.2	**FE-1**	2	0.9
FX-4	1	0.4	**FX-4**	2	1.4
G-I	1	0.5	**G-I**	2	0.7
	MEAN	1.0		**MEAN**	1.4

Table 3. Hydro-geomechanical characteristics of the aquifers and aquitard in Manzanares-Jarama wellfield.

Aquifer/aquitard		Kxx (m/s)	Kyy (m/s)	Kzz (m/s)	S_s (1/m)	E (MPa)
Shallow aquifer	Initial value	6.00×10^{-7}	6.00×10^{-7}	3.00×10^{-8}	1.00×10^{-5}	82.5
	Calibrated value	6.00×10^{-7}	6.00×10^{-7}	3.00×10^{-8}	3.00×10^{-6}	247.6

Aquitard	Initial value	2.00×10^{-10}	2.00×10^{-10}	1.00×10^{-11}	1.00×10^{-5}	82.5
	Calibrated value	2.00×10^{-10}	2.00×10^{-10}	1.00×10^{-11}	1.00×10^{-5}	82.5
Deep aquifer	Initial value	3.40×10^{-7}	3.40×10^{-7}	1.70×10^{-8}	1.00×10^{-5}	82.5
	Calibrated value	1.85×10^{-5}	1.85×10^{-5}	5.00×10^{-6}	3.00×10^{-6}	247.6

Table 4. Average absolute error and standard deviation between the simulated hydraulic head changes and the observed measurements at the piezometers. The error percentage computed considering the maximum drawdown during the groundwater extraction cycles is also reported for each piezometer.

Piezometers	Maximum drawdown of the groundwater extraction cycles (m)	Average absolute error (m)	Standard deviation (m)	Percentage of error (%)
FA-1	116.67	8.46	7.57	7.25
FA-3	123.44	10.24	9.17	8.30
FX-4	118.51	9.56	10.41	8.06
FC-2	117.86	10.59	9.79	8.98
FE-1	117.02	11.22	9.29	9.59
G-I	148.15	25.95	11.28	17.51
CA-5	130.17	8.46	8.46	6.50
CA-4	136.81	8.51	7.39	6.22
CA-3	107.68	10.21	11.78	9.48
CB-15	102.48	6.86	7.13	6.69
CB-14	115.25	6.76	6.54	5.87
CB-13	112.18	7.70	7.54	6.87
CB-12	85.10	8.85	8.50	10.40
CB-11	121.64	9.23	9.68	7.59
CB-9	134.04	19.10	10.73	14.25
CB-6	193.23	18.25	14.66	9.45
CB-5	146.15	16.30	14.14	11.15

Figures
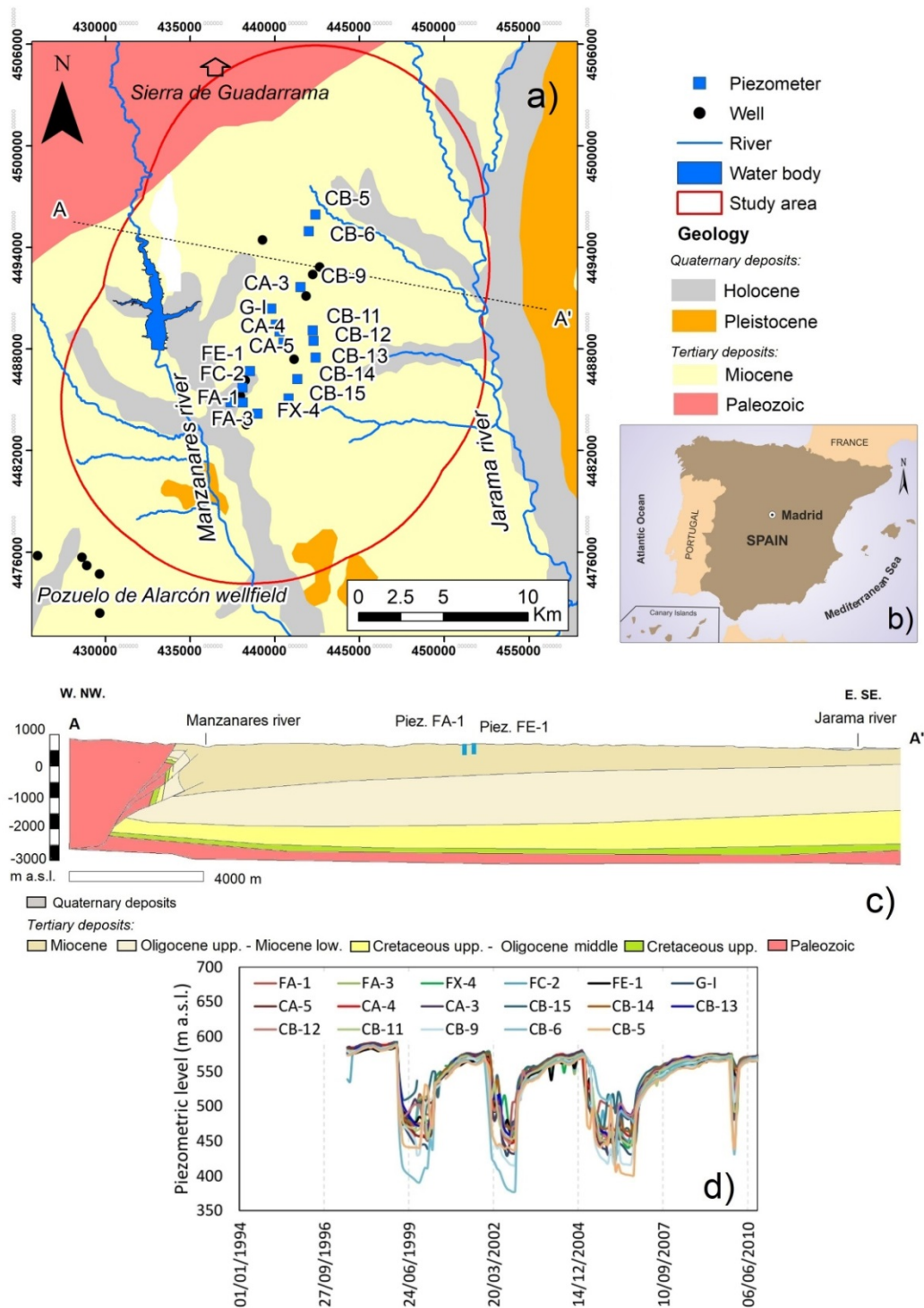
Figure 1. (**a**) Geological map (IGME, 1995) with the location of piezometers and wells of the Manzanares-Jarama wellfield and the trace of the main water bodies and the rivers (derived from https://servicio.mapama.gob.es/sia/visualizacion/descargas/mapas.jsp). (**b**) Geographical location of the of the study area in Spain. (**c**) Geological cross-section modified from IGME (2000). (**d**) Time series of the piezometric head recorded on the 17 piezometers located in the wellfield. The coordinate system of the data is European Datum 1950 (ED 1950 UTM Zone 30N).
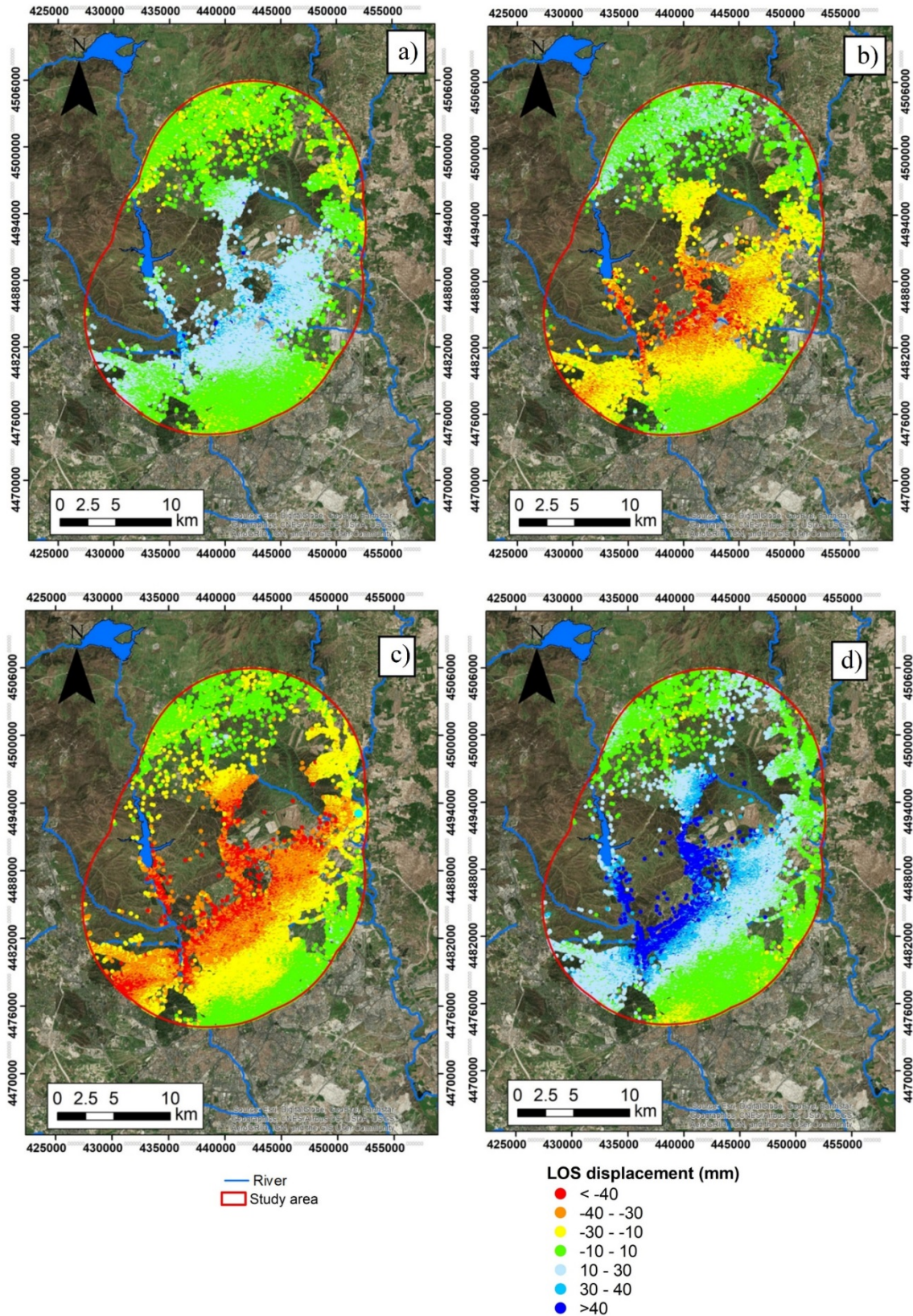
Figure 2. LOS displacements (mm) during different recovery and extraction periods: (**a**) from January 1996 to January 1999, (**b**) from February 1999 to March 2000, as measured using the ERS-1/2 data acquired along the descending mode; and (**c**) from April 2005 to October 2006, (**d**) from December 2006 to September 2010, as measured using ENVISAT data acquired along the ascending mode.
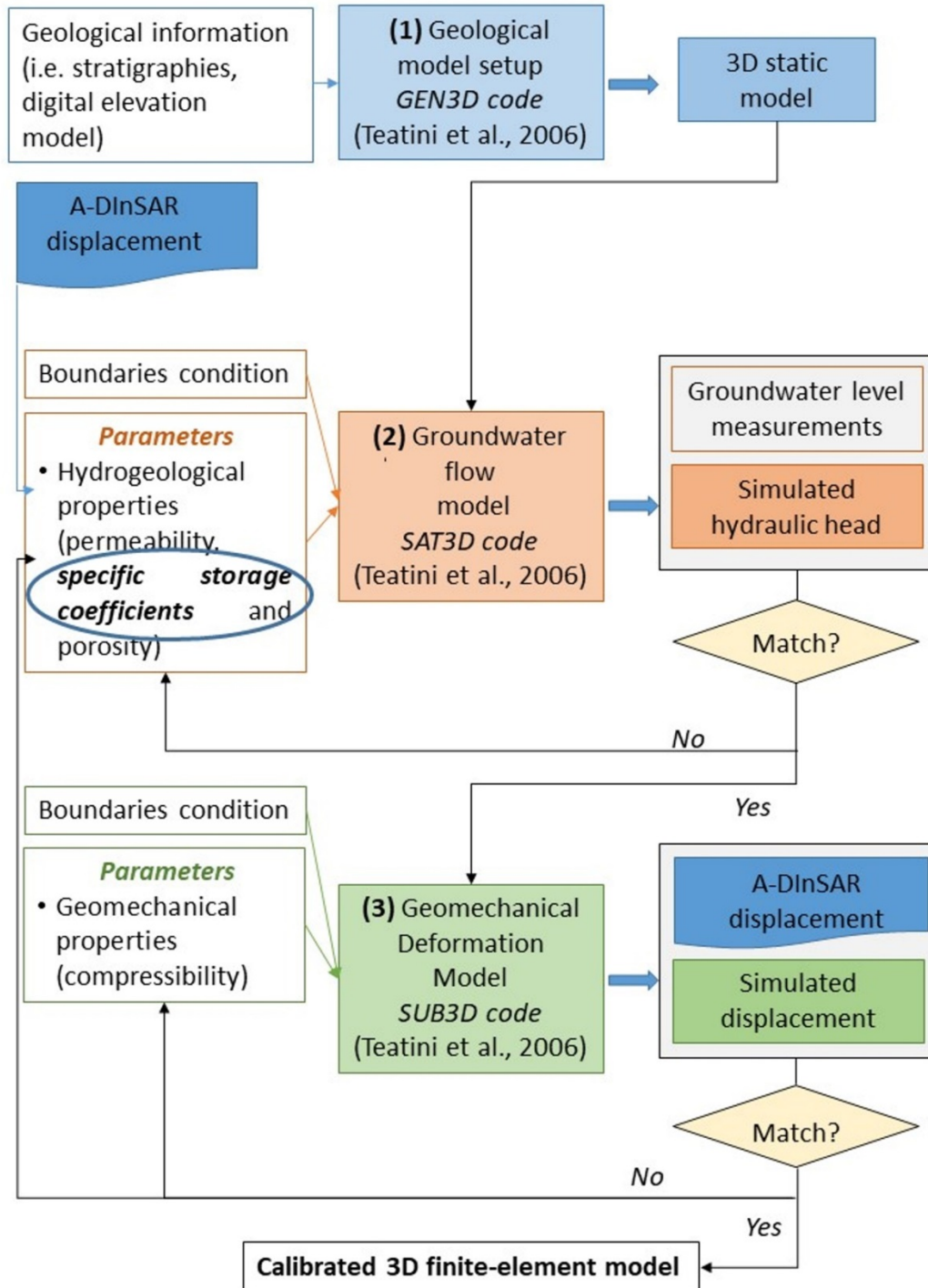
Figure 3. Flowchart of the methodological approach for the calibration of the 3D modelling approach.
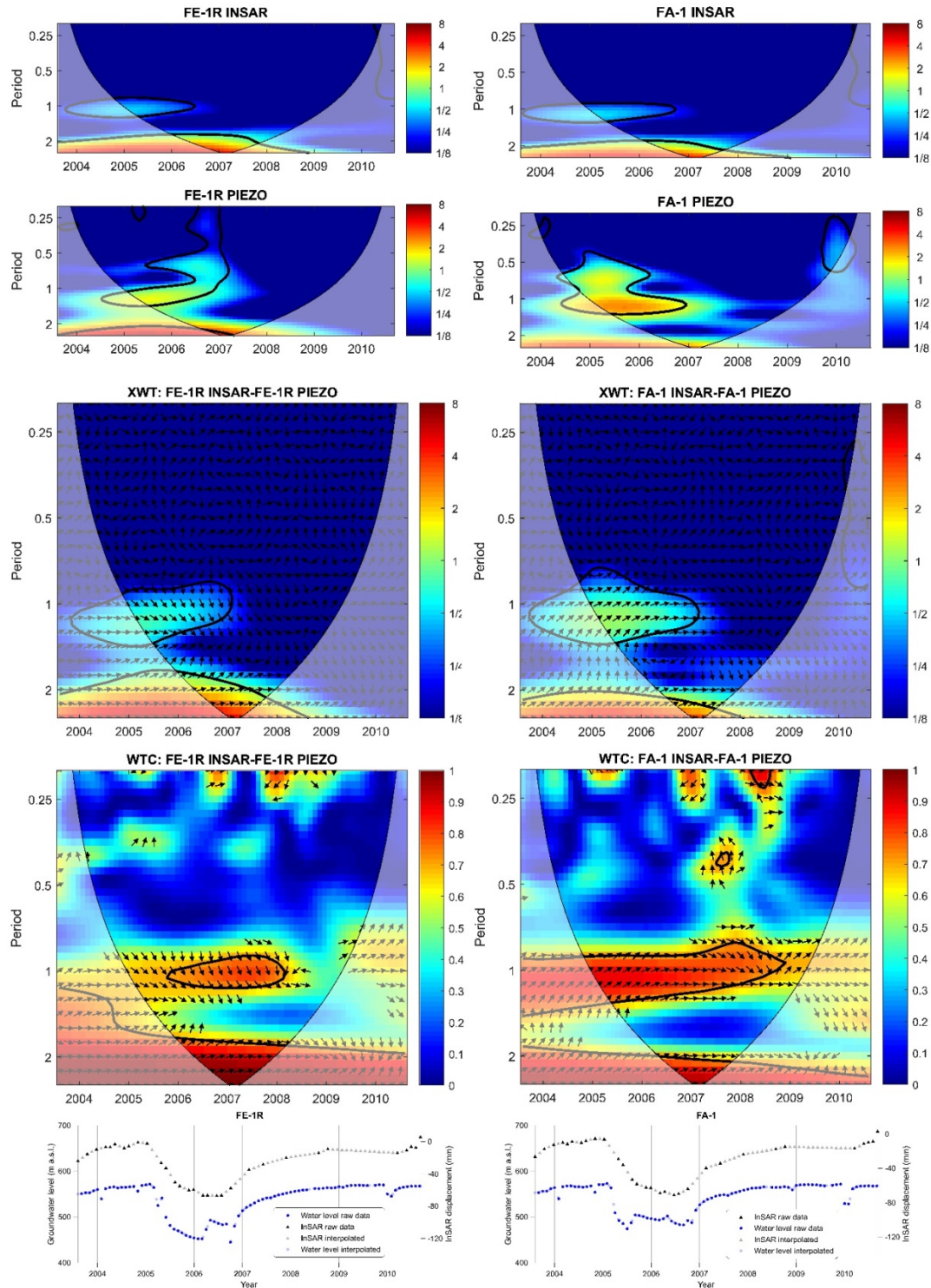
Figure 4. Example of wavelet scalograms. CWT of A-DInSAR displacement and piezometric level time series, respectively, in the well FE-1 and FA-1; XWT and WTC of both time series. For each scalogram, x-axis represents the time space and y-axis the scale space (in Fourier periods). The thick contour reported in the scalograms designates the 5% significant level against the Brownian noise. The cone of influence where edge effects might distort the picture is shown as a lighter shadow. The colour bars of CWT and XWT represent the wavelet power of individual time series and the common cross-wavelet power of both time series, respectively, ranging from blue (low) to red (high). Coherency of WTC ranges from blue (low) to red (high). The relative phase relationship is shown as arrows (with in-phase pointing right and anti-phase pointing left).
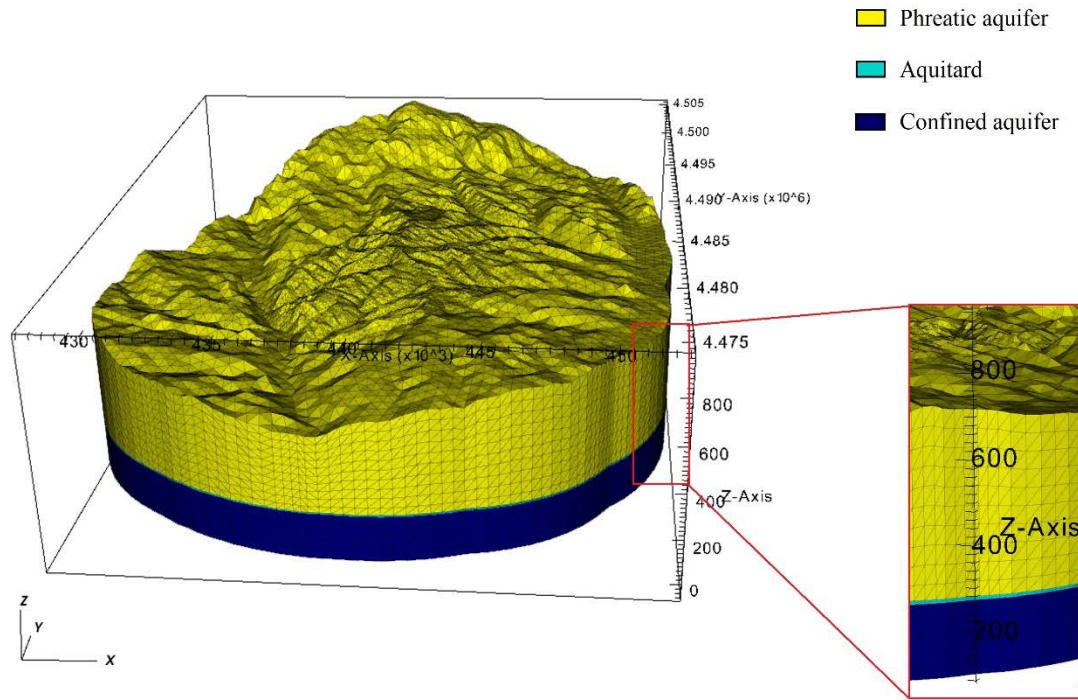
Figure 5. 3D hydrogeological model of the Manzanares-Jarama wellfield. The aquitard thickness is equal to 10 m.
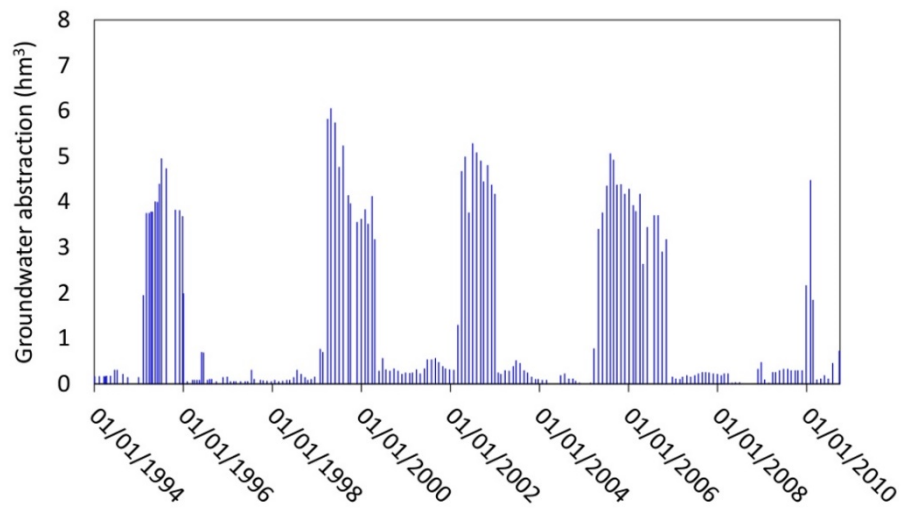
Figure 6. Monthly groundwater withdrawal during the period between 1994 and 2010 addressed by the analyses developed in this study.
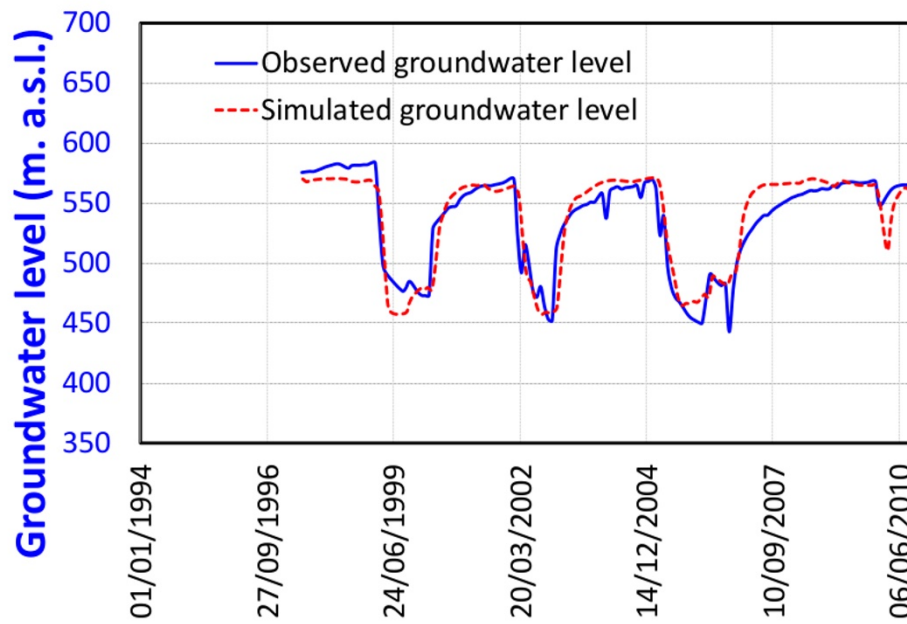
Figure 7. Cycles of piezometric decline and natural recovery as recorded at piezometer FE-1 and computed by the SAT3D groundwater flow simulator. The piezometers FE-1 is representative of the groundwater level variations observed in the wellfield (Figure 1a).
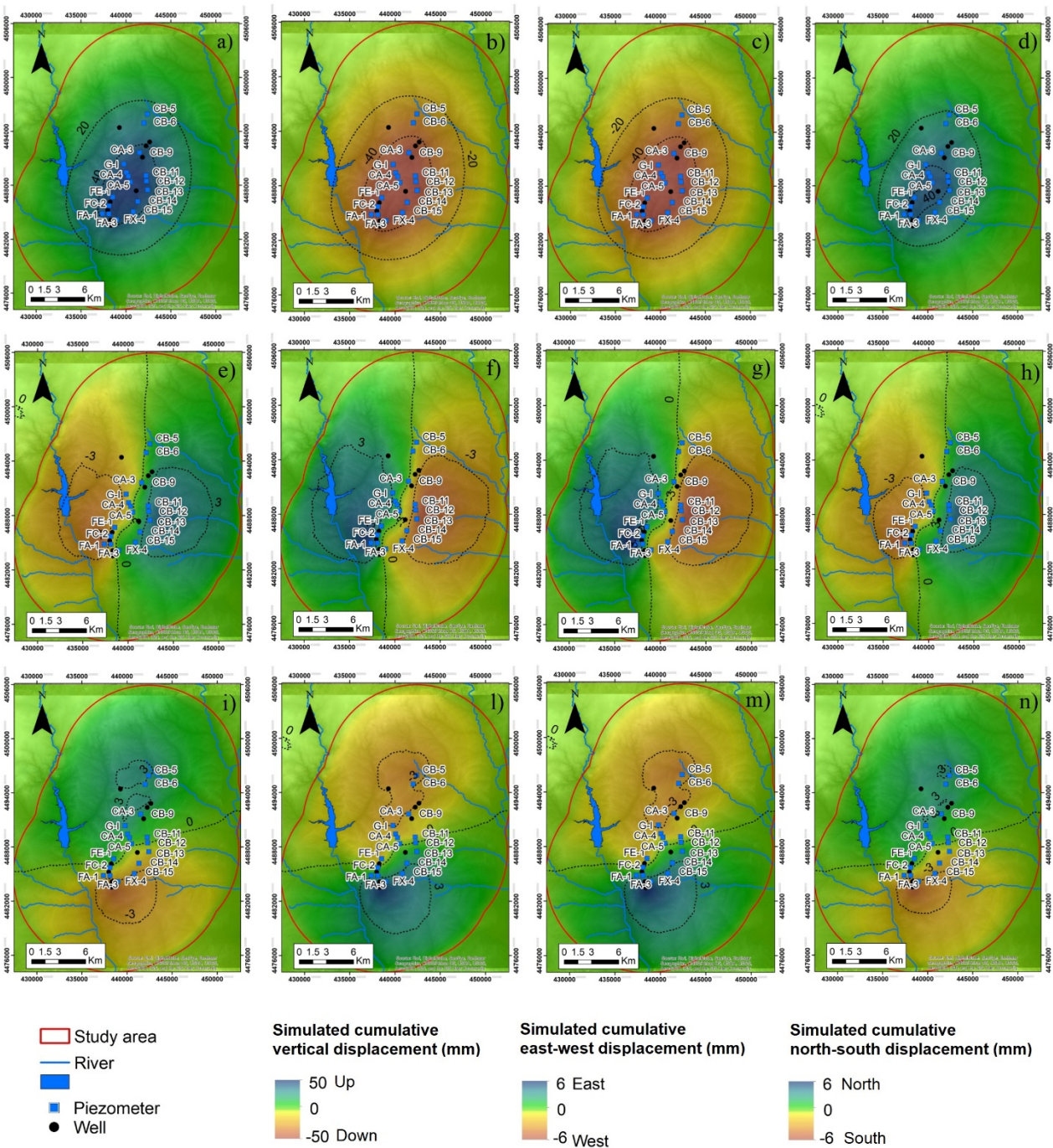
Figure 8. Simulated displacements in a few representative periods: (**a**) from January 1996 to January 1999, (**b**) from February 1999 to March 2000, (**c**) from April 2005 to October 2006, (**d**) from December 2006 to September 2010. The computed displacements along the (**e, f, g** and **h**) west-east and (**i, l, m** and **n**) south-north directions are provided for the same periods.
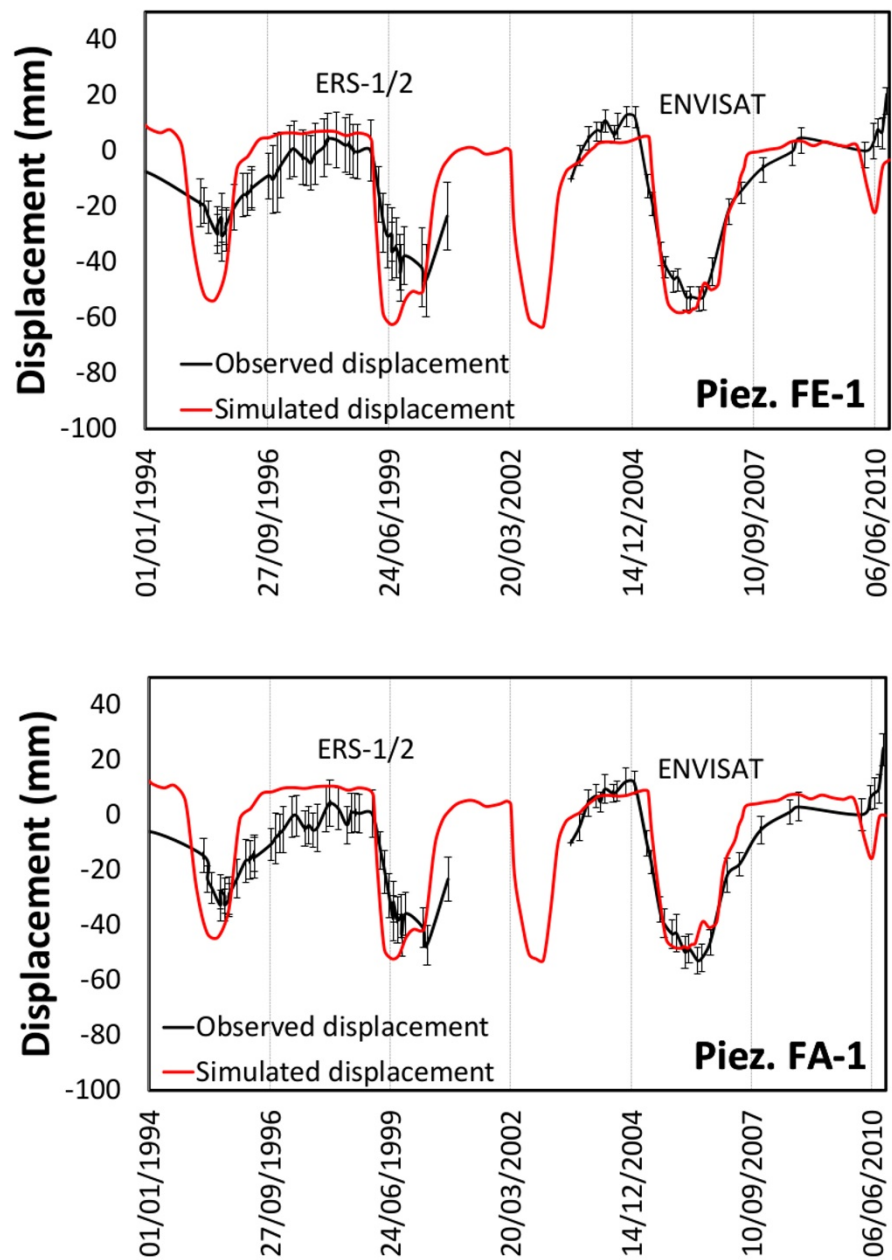
Figure 9. Simulated and observed vertical displacement at piezometers FE-1 and FA-1. See the location of the piezometers in Figure 1. It is worth noting that the observed vertical displacements represent an average value within a buffer zone of 1000 m from the wells, therefore also the standard deviation is reported.
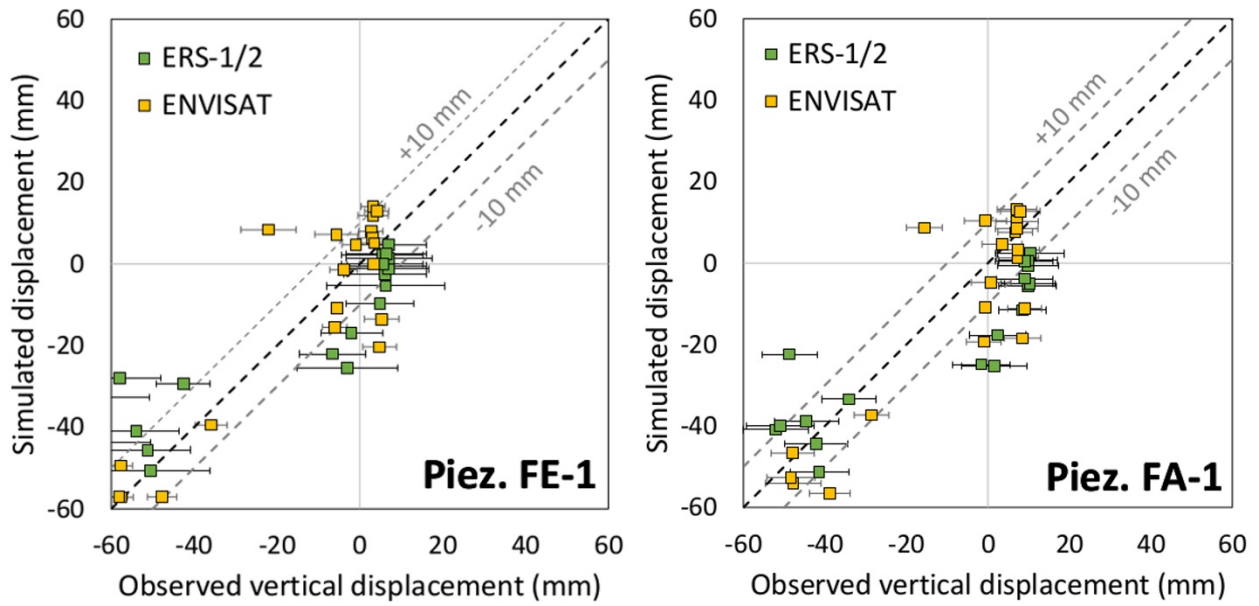
Figure 10. Simulated vertical displacement plotted versus the observed vertical measurements obtained using A-DInSAR technique at piezometers FE-1 and FA-1. The standard deviation of the observed displacements is also reported.
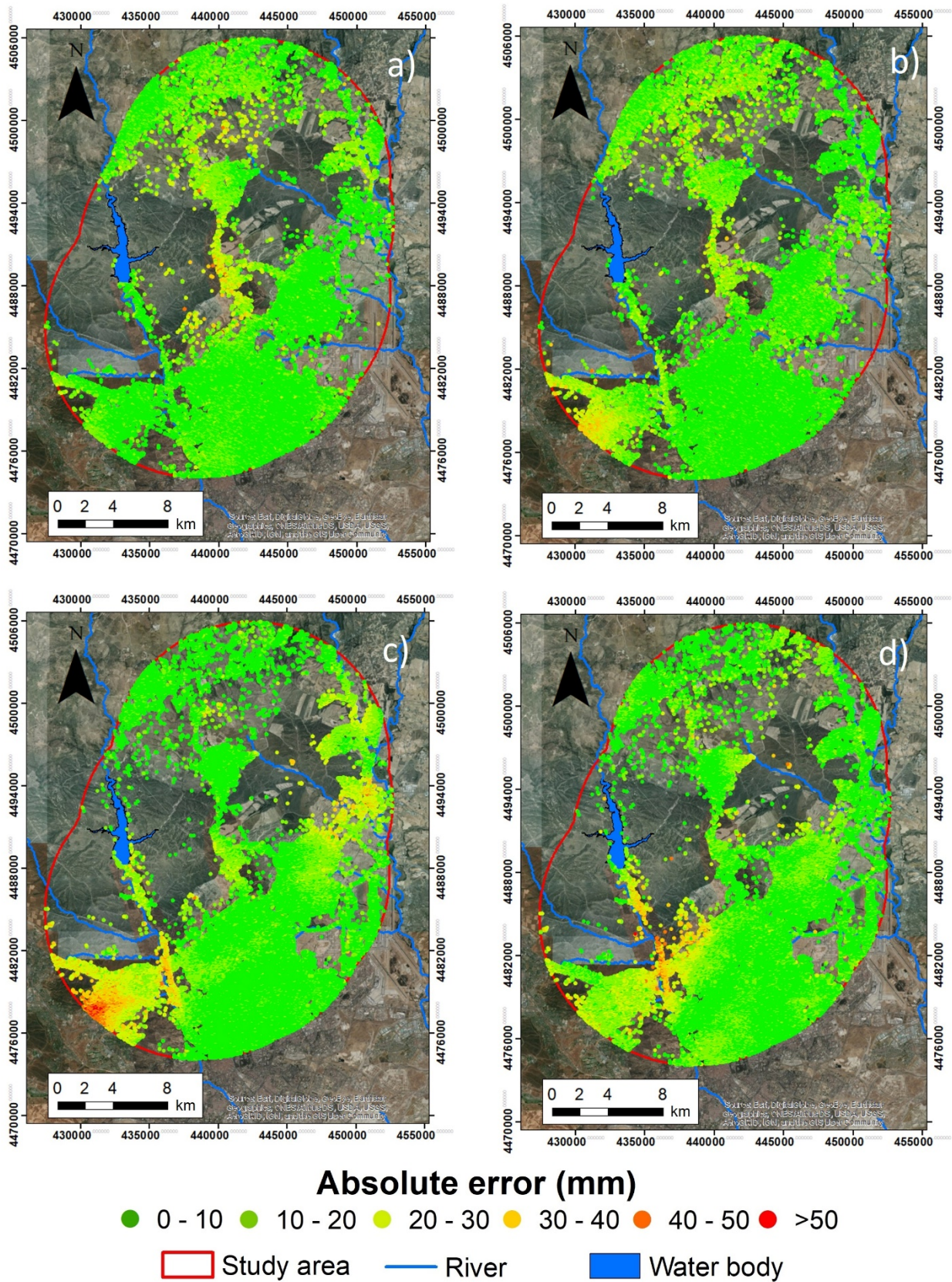
Figure 11. Absolute error between the measured and simulated land displacements during few recovery and withdrawal periods: (**a**) from January 1996 to January 1999; (**b**) from February 1999 to March 2000; (**c**) from April 2005 to October 2006; and (**d**) from December 2006 to September 2010.
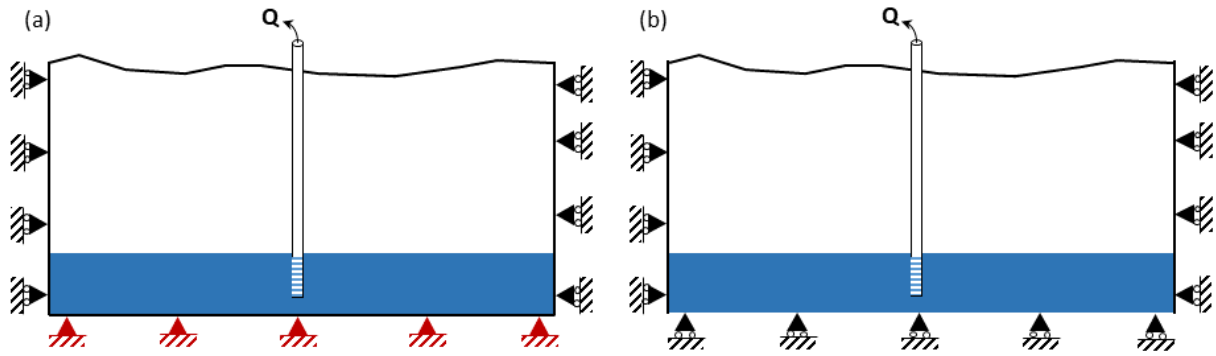
Figure 12. Sketch representing the boundary conditions used in the 3D geomechanical model: (**a**) type 1 setting, (**b**) type 2 setting.
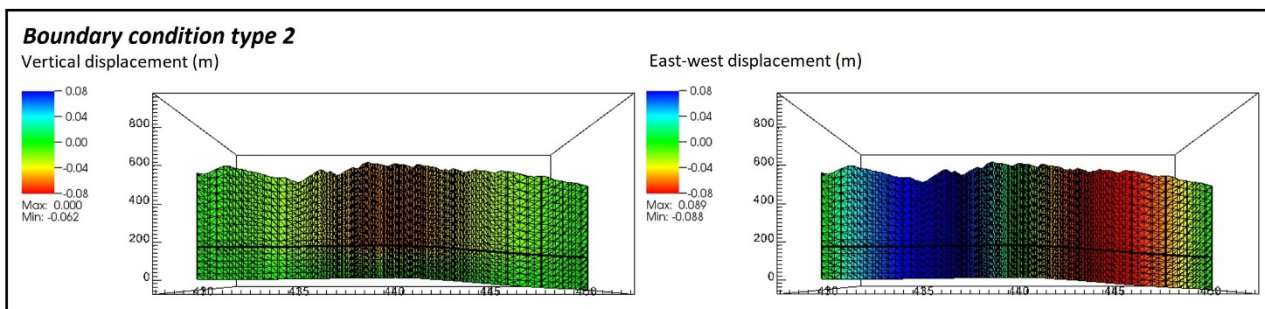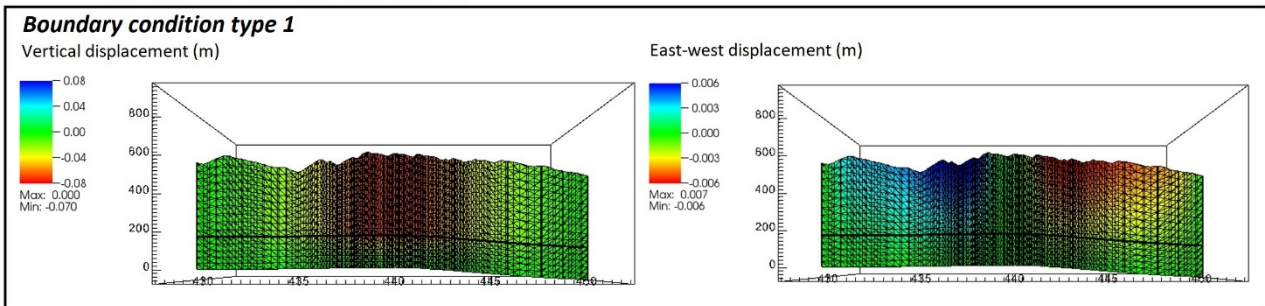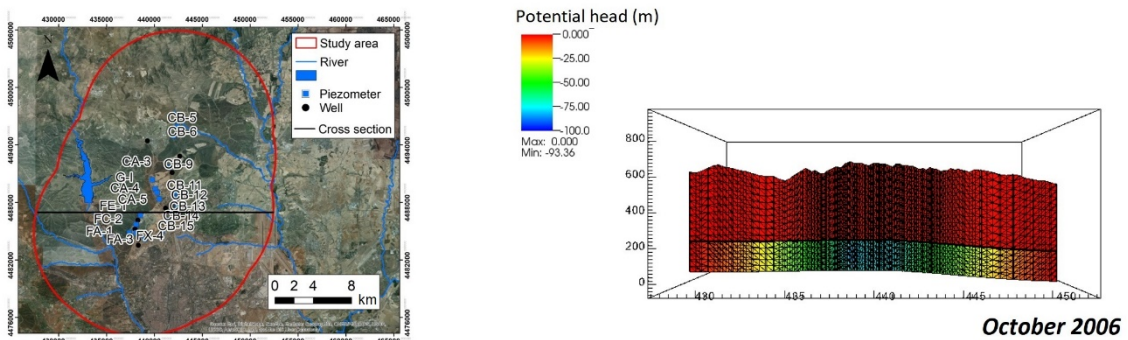

Figure 13. West-east cross section of the model showing the pattern of the piezometric change in October 2006 (at the end of the groundwater abstraction period) and the vertical and horizontal (west-east) displacements as obtained using the two types of boundary conditions on the domain bottom.
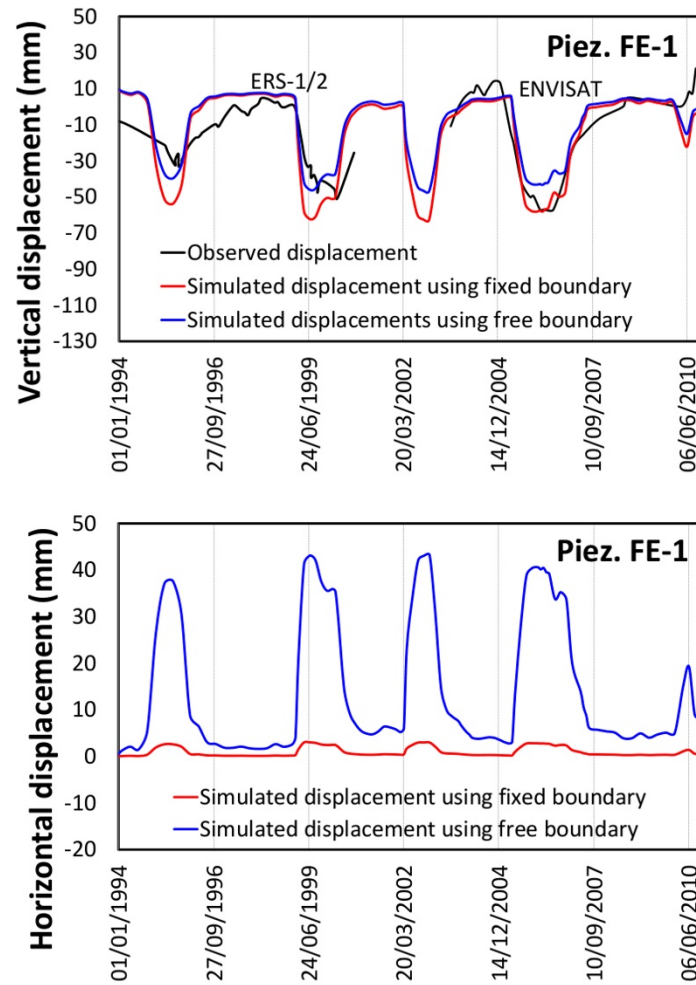
Figure 14. (**a**) Comparison between the measured and the simulated vertical displacements computed at piezometer FE-1. The model outcomes refer to the two types of boundary conditions on the model bottom. (**b**) Horizontal (west-east) displacements obtained by the geomechanical model using the different boundary conditions at the same FE-1 location.